NAVAL POSTGRADUATE SCHOOL

MONTEREY, CALIFORNIA

THESIS

MULTISTATIC RADAR IMAGING FOR MOVING TARGETS

by

Ng Chee Yong

December 2009

Thesis Advisor:	Brett H. Borden
Second Reader:	Phillip E. Pace

Approved for public release; distribution is unlimited

REPORT DOCUMENTATION PAGE			Form Approved OMB No. 0704-0188
Public reporting burden for this collection of information is estimated to average 1 hour per response, including the time for reviewing instruction, searching existing data sources, gathering and maintaining the data needed, and completing and reviewing the collection of information. Send comments regarding this burden estimate or any other aspect of this collection of information, including suggestions for reducing this burden, to Washington headquarters Services, Directorate for Information Operations and Reports, 1215 Jefferson Davis Highway, Suite 1204, Arlington, VA 22202-4302, and to the Office of Management and Budget, Paperwork Reduction Project (0704-0188) Washington DC 20503.			
1. AGENCY USE ONLY *(Leave blank)*	**2. REPORT DATE** December 2009	**3. REPORT TYPE AND DATES COVERED** Master's Thesis	
4. TITLE AND SUBTITLE Multistatic Radar Imaging for Moving Targets		**5. FUNDING NUMBERS**	
6. AUTHOR(S) Ng Chee Yong			
7. PERFORMING ORGANIZATION NAME(S) AND ADDRESS(ES) Naval Postgraduate School Monterey, CA 93943-5000		**8. PERFORMING ORGANIZATION REPORT NUMBER**	
9. SPONSORING /MONITORING AGENCY NAME(S) AND ADDRESS(ES) N/A		**10. SPONSORING/MONITORING AGENCY REPORT NUMBER**	
11. SUPPLEMENTARY NOTES The views expressed in this thesis are those of the author and do not reflect the official policy or position of the Department of Defense or the U.S. Government.			
12a. DISTRIBUTION / AVAILABILITY STATEMENT Approved for public release; distribution is unlimited		**12b. DISTRIBUTION CODE**	

13. ABSTRACT (maximum 200 words)

In this thesis, we study the new imaging theory developed by *Cheney* and *Borden* [1] that incorporates target motion during data collection for the imaging process. The subject of radar imaging from scattered waves is explored and incorporated into the new imaging approach. A simulation model using MATLAB is developed to simulate the imaging algorithm and also to validate the performance. It is shown that the new imaging scheme is well behaved and is linear shift invariant when the data are ideal. It is also shown that the geometry of the transmitters and receivers affects the behavior of the imaging system.

14. SUBJECT TERMS Radar Imaging, Moving Targets, Point Spread Function, Ambiguity Function			**15. NUMBER OF PAGES** 85
			16. PRICE CODE
17. SECURITY CLASSIFICATION OF REPORT Unclassified	**18. SECURITY CLASSIFICATION OF THIS PAGE** Unclassified	**19. SECURITY CLASSIFICATION OF ABSTRACT** Unclassified	**20. LIMITATION OF ABSTRACT** UU

NSN 7540-01-280-5500 Standard Form 298 (Rev. 2-89)
Prescribed by ANSI Std. 239-18

THIS PAGE INTENTIONALLY LEFT BLANK

Approved for public release; distribution is unlimited

MULTISTATIC RADAR IMAGING OF MOVING TARGETS

Ng Chee Yong
Defence Science and Technology Agency, Singapore
Bachelor of Engineering (Electrical and Electronics Engineering),
Nanyang Technological University of Singapore, 2003

Submitted in partial fulfillment of the
requirements for the degree of

MASTER OF SCIENCE IN COMBAT SYSTEMS TECHNOLOGY

from the

NAVAL POSTGRADUATE SCHOOL
December 2009

Author: Ng Chee Yong

Approved by: Brett H. Borden
Thesis Advisor

Phillip E. Pace
Second Reader

Andres Larraza
Chairman, Department of Physics

THIS PAGE INTENTIONALLY LEFT BLANK

ABSTRACT

In this thesis, we study the new imaging theory developed by *Cheney* and *Borden* [1] that incorporates target motion during data collection for the imaging process. The subject of radar imaging from scattered waves is explored and incorporated into the new imaging approach. A simulation model using MATLAB is developed to simulate the imaging algorithm and also to validate the performance. It is shown that the new imaging scheme is well behaved and is linear shift invariant when the data are ideal. It is also shown that the geometry of the transmitters and receivers affects the behavior of the imaging system.

THIS PAGE INTENTIONALLY LEFT BLANK

TABLE OF CONTENTS

LIST OF FIGURES

ACKNOWLEDGMENTS

I am thankful to Professor Brett Borden, my thesis professor, for his guidance and patience throughout my study at the Naval Postgraduate School. He was encouraging and supportive throughout my thesis work. He has made this thesis very meaningful to me by explaining the complex concept and made it insightful and enjoyable. I would also like to thank the co advisor, Professor Phillip Pace for providing many insightful comments that have contributed to my learning and clarity of this thesis. Last but not least, to my wife, Tessa, and my son, Josiah, for their support and strength throughout this endeavor.

THIS PAGE INTENTIONALLY LEFT BLANK

I. INTRODUCTION

A. RADAR IMAGING

Radar is a system that uses electromagnetic waves for detecting, locating, and identifying reflecting objects over long distances in both adverse and good weather conditions. Unlike optical systems, radar systems are generally not affected by atmospheric attenuation because of the wavelengths used. However, in imaging, the resolution of the image is dependent on the signal wavelength. Although radar-based imaging systems have coarser resolution than other types of imaging systems, many objects of interest are still within the ranges of the signal wavelength employed by radar systems.

Many radar imaging techniques have been developed since the 1950s to improve the resolution of radar-based imaging systems. Examples of such techniques are Synthetic Aperture Radar (SAR) and the Inverse Synthetic Aperture Radar (ISAR), which have the ability to produce imagery with high resolution.

B. IMAGING TECHNIQUES TO CREATE ARTIFACT FREE IMAGERY

The main goal in radar-based imaging techniques is to create an artifact free image. Model assumptions are used for traditional imaging techniques; however, these assumptions indirectly cause the image artifacts as discussed in the literature. The start-stop approximation is common to all existing imaging techniques and this is central to the thesis and holds a fundamental difference between the new imaging scheme developed in [1] and current techniques.

1. The Born Approximation

In the standard radar scattering model, an object is assumed to be composed of a collection of simple point scatterers. When considering multiple scattering (in which the scatterers are allowed to interact) analysis becomes too unwieldy. Hence the “weak

scatterer" or Born approximation is used instead. This approximation treats the scatterers as non-interacting and results in a more manageable linear problem. However, with the Born approximation, image artifacts may still exist, as this approximation discards the higher order multiple-scattering terms.

2. Bandwidth Limited Radar Systems

Although, ideally, an infinite bandwidth is desired, all practical systems are bandwidth-limited, and this fact affects image resolution. In addition, the signal information measured from practical systems is not noise-free, as it is always corrupted by unwanted signals, and this also causes unwanted image artifacts.

3. The "Start-Stop" Approximation

Most modern radar systems use a train of pulses together with coherent integration for the detection of a target and for an estimation of the target's velocity. These types of waveforms typically allow the use of the start-stop approximation, which assumes the target is stationary during the measurement process. This is a reasonable approximation, since the speed of the target is relatively slow when compared to the speed of the electromagnetic waves, which travel at the speed of light. By this approximation, velocity estimates are based on range change-rate. Target position and closing speed can be estimated from the measured range and range-rate obtained during the measurement process.

In order to achieve better signal-to-noise ratio (SNR) in the measurements, coherent integration is required. However this can require significant number of pulses in the pulse train. When the pulse train gets too long, the stationary target approximation may not be valid. The target may move considerably within the pulse interval of the pulse train, which may result in a blurred range.

C. MOTIVATION: IMAGING MOVING TARGETS

Many imaging techniques have been developed to image moving targets. For example the Space-Time Adaptive Processing (STAP) (which is a signal processing technique) uses multiple-element antenna arrays coupled with real-aperture imaging techniques to produce ground moving target indicator (GMTI) images [2]. The technique described in [3] uses SAR (designed to image stationary scenes) together with GMTI processing for detecting slow-moving surface targets that exhibit start-stop like maneuvers. Another method described in [4] discusses an implementation based on forward looking array radar.

Velocity Synthetic Aperture Radar (VSAR) is another approach and is described in [5]. VSAR is a multi-element SAR system that uses conventional processing to form an image for each element (or sub-array). The image phases are preserved and compared to estimate the target velocity. However, this method assumes that the scatterers remain in a resolution cell throughout the measurement period.

There is a common assumption made by these imaging techniques: namely that the target is instantaneously stationary while it interacts with the wave. Therefore, there is generally some need for an imaging technique that can accommodate target motion in a more complete way. This is the main focus of this thesis.

D. OBJECTIVE

The objective of this thesis is to study a linearized imaging theory, developed by Professors Cheney and Borden [1], for imaging a scene with moving targets. The physics behind it and the approach to address image artifacts associated with targets moving in an unknown fashion will be discussed. There will be analysis of a new imaging code based on a moving point scatterer via MATLAB simulation. The behavior of the imaging model will also be examined under different data collection geometries.

THIS PAGE INTENTIONALLY LEFT BLANK

II. IMAGING THEORY

In this chapter, we discuss how a radar system obtains range and Doppler information of a target and how radar images are formed. We also discuss the problems associated with radar imaging and its challenges.

A. RADAR SYSTEMS

Radar systems use electromagnetic waves to detect the presence of a target in an area of interest. These systems send out a signal, which could be a pulse or a series of pulses (known as pulse train), and this signal interacts with a target and is reflected back to the radar. From the reflected signal, the two measurements that can be obtained are the round trip time delay of the transmitted signal and the target radial velocity. The range of the target is determine by measuring the round trip time delay, τ, where Range, $R = c\tau / 2$. The radical velocity can be obtained from the phase change of the reflected signal compared to the transmitted signal.

The down range resolution of the radar system is determined by the pulse bandwidth. The transmitting frequencies are usually 20 GHz and below, as the atmospheric attenuation of waves with these frequencies is negligible. Higher frequencies are subject to higher atmospheric attenuation. However, there are gaps at some ranges among the higher frequencies that have lesser attenuation and could be exploited for various requirements. Systems with large bandwidth are capable of producing a finer down range resolution, and such systems are typically sought for imaging or identification purposes.

B. SCATTERING OF ELECTROMAGNETIC WAVES

Radar information is based on the reflected electromagnetic waves. Understanding the behavior and properties of such waves provides important information about the target.

From the discussion in [6], a one-dimensional scattering model for a moving PEC[1] plate in free space is commonly used as an illustration. Assuming the waveform generator produces a time varying waveform $s(t)$ and is mixed with the carrier wave of frequency w_0 to produce $f(t) = s(t)\cos(w_0 t)$, the transmitted field is,

$$\tilde{E}_{inc}(x,t) = \tilde{E}_0^{inc} f(t - x/c) \tag{2.1}$$

With the transmitted wave propagating along the *x*-axis, we expect the scatter field to be propagating in the opposite direction, which is along the $-$x-axis and can be expressed as,

$$\tilde{E}_{scatt}(x,t) = \tilde{E}_0^{scatt} g(t + x/c) \tag{2.2}$$

Further assuming the position of the plate is $x = R(t)$, the boundary condition on the PEC for the scattered field is,

$$\tilde{E}_{scatt} g(t + R(t)/c) = -\tilde{E}_{inc} f(t - R(t)/c) \tag{2.3}$$

For simplicity, assuming that the plate undergoes linear motion so that $R(t) = x + vt\Big|_{x=R(\text{at boundary})}$, where v is the rate the range changes and is also known as the range-rate. For short pulses, $R(t) = x + vt$ can be considered to be the first two terms of Taylor expansion (valid for small t). Substituting, $u = t + R(t)/c$, we can solve for t in terms of u (at boundary condition):

$$t = \frac{u - R/c}{1 + v/c} \tag{2.4}$$

and so the scattered field can be expressed as:

$$\tilde{E}_{scatt}\, g(t + R(t)/c) = -\tilde{E}_{inc}\, f\left[\alpha(t + x/c - R/c) - R/c\right] \tag{2.5}$$

where the Doppler scale factor α is:

[1] A perfect electrical conductor (PEC) allows the charges to move freely and instantaneously in response to a field and the fields inside a PEC are zero. The boundary conditions are that the tangential components of the electric field must be zero and the tangential components of the magnetic field are related to currents flowing on the surface of the PEC.

$$\alpha = \frac{1 - v/c}{1 + v/c} \tag{2.6}$$

Since the transmitted waveform is f(t) = $s(t)\cos(\omega_0 t)$, the scattered signal obtained at the antenna (x = 0) is:

$$p_{rec}(t) = f[\alpha(t - R/c) - R/c] = s[\alpha(t - R/c) - R/c]\cos[w_0(\alpha(t - R/c) - R/c)] \tag{2.7}$$

for a scatterer that is slowly varying so that v/c is small. We can expand the denominator of Equation (2.6) in a geometric series to obtain

$$\alpha = (1 - v/c)(1 - v/c + \mathrm{O}[(v/c)^2] = 1 - 2v/c + \mathrm{O}[(v/c)^2] \tag{2.8}$$

approximating $\alpha \approx 1 - 2v/c$, we can approximate the argument $\alpha(t - R/c) - R/c \approx t - 2R/c$ to obtain

$$p_{rec}(t) \approx s(t - 2R/c)\cos\left(\omega_0\left[(1 - 2v/c)(t - R/c) - R/c\right]\right) \tag{2.9}$$

It can be seen that the carrier frequency has been shifted by an amount,

$$\omega_D = -\frac{2v}{c}\omega_0 \tag{2.10}$$

This is known as the Doppler shift. If the target moves towards the antenna (v < 0), then the Doppler shift is positive. If the target moves away from the antenna (v > 0), then the Doppler shift is negative. Although radar targets are not usually made of PEC plates, the received signal is nevertheless well modeled as a time delayed and Doppler-shifted version of the transmitted signal. This model is valid for most targets.

C. CORRELATION RECEPTION

From the radar range equation [7], it is easily seen that the received signal is reduced in energy by a factor of R^{-4} of the transmitted signal. Larger detection ranges can be achieved by increasing the transmitted power of the signal; however the transmitter power is usually limited by operational requirements. It is common for the receiver of the radar to be expected to detect a signal power as low as 10^{-18} Watts.

Although we can easily increase the signal to noise ratio (SNR) by doing coherent pulse integration, there are limitations. For example, the increase of pulse repetition frequency will also decrease the maximum unambiguous range. The target usually moves during data collection, which results in the phase of the scattered field being altered. Pulse integration is also limited by the ability of the local oscillator to remain coherent over the interval in which the pulses are transmitted.

Radar obtains information about a target by comparing the received signal with the transmitted signal. In such processing, the objective is to separate the scattered field from the random noise contamination in the received signal $s_{rec}(t)$.

$$s_{rec}(t) = s_{scatt}(t) + n(t) \tag{2.11}$$

Maximum likelihood processing selects the best estimate for the scattered field, which maximizes the probability of scattered signal $s_{scatt}(t)$ for a given $s_{rec}(t)$ over all time. From [6], it is shown that such processing, averaged over all time reduces to the problem of finding a function $s_{scatt}(t)$ that minimizes:

$$\int_{-\infty}^{\infty} \left|s_{rec}(t')\right|^2 dt' + \int_{-\infty}^{\infty} \left|s_{scatt}(t')\right|^2 dt' - 2\,\mathrm{Re}\int_{-\infty}^{\infty} s_{rec}(t')s_{scatt}^{*}(t')dt' \tag{2.12}$$

Searching for the best minimizing function is made more efficient by restricting the search to a few parameters. In this case, the natural model is based on the scattering interaction between the interrogating field and the target. If $s_{inc}(t)$ denotes an incident pulse transmitted by the radar, then the linear radar (weak-scatterer) scattering model follows by superposition

$$s_{scatt}(t) = \iint_{-\infty}^{\infty} \rho(\upsilon,\tau)s_{inc}(t-\tau)e^{i\upsilon(t-\tau)}d\tau d\upsilon \tag{2.13}$$

where $\rho(\upsilon,\tau)$ is the target reflectivity density defined such that $\rho(\upsilon,\tau)d\tau d\upsilon$ is proportional to the field reflected from the target at range between $c\tau/2$ and $c(\tau+d\tau)/2$ with Doppler shift between υ and $\upsilon+d\upsilon$.

From Equation (2.13) , the target reflectivity scattered field is dependent on the two parameters τ and υ. The parameters for the simplest search space would be the time shift τ and the Doppler shift υ. The correlation receiver tries to find τ and υ which maximize the real part of:

$$\eta(\upsilon,\tau)=\int_{-\infty}^{\infty} s_{rec}(t')s_{inc}^{*}(t'-\tau)e^{-i\upsilon(t'-\tau)}dt' \tag{2.14}$$

The real part of the correlation integral output will be maximum when the received signal "looks-like" a time-delayed and frequency-shifted version of the transmitted signal. Other signals, like noise from the receiver circuit and the environment, will be suppressed. As such, the correlation receiver appears to be operating like a type of "matched filter".

By substituting Equation (2.13) into Equation (2.14), the output of the correlation receiver results in

$$\eta(\upsilon,\tau)=\iint_{-\infty}^{\infty} \rho(\upsilon',\tau')\chi(\upsilon-\upsilon',\tau-\tau')e^{i\frac{1}{2}(\upsilon+\upsilon')(\tau-\tau')}d\tau'd\upsilon' \tag{2.15}$$

where

$$\chi(\upsilon,\tau)=\int_{-\infty}^{\infty} s_{inc}(t')s_{inc}^{*}(t'+\tau)e^{i\upsilon t'}dt' \tag{2.16}$$

The correlation noise term is considered to be very small as compared to the signal of interest, and hence it is not explicitly displayed in the Equation. The standard radar data model is shown in Equation (2.15), and it expresses the output of the correlation receivers as a convolution of ρ and χ. The function $\chi(\upsilon,\tau)$ as defined in Equation (2.16) is also known as the ambiguity function.

D. ONE-DIMENSIONAL (HIGH RANGE RESOLUTION) IMAGING

In general, radar pulses are often of short duration and target velocity is almost stationary when compared to the speed of light. These short pulse signals can be used to form one-dimensional high range resolution (HRR) "images" of the target. This method

works when the transmitted pulse's instantaneous range resolution is smaller than the size of the target. When the scattering of the sub-elements of the target are non-interacting and point-like, the scattered pulse will be a sum of the damped and blurred images of the incident pulse, which are shifted by time-delays that are proportional to the sub-element's range [8]. Figure 1 shows a one-dimensional image created by an HRR radar system. It is clearly shown that the peak profiles are associated with isolated target elements.

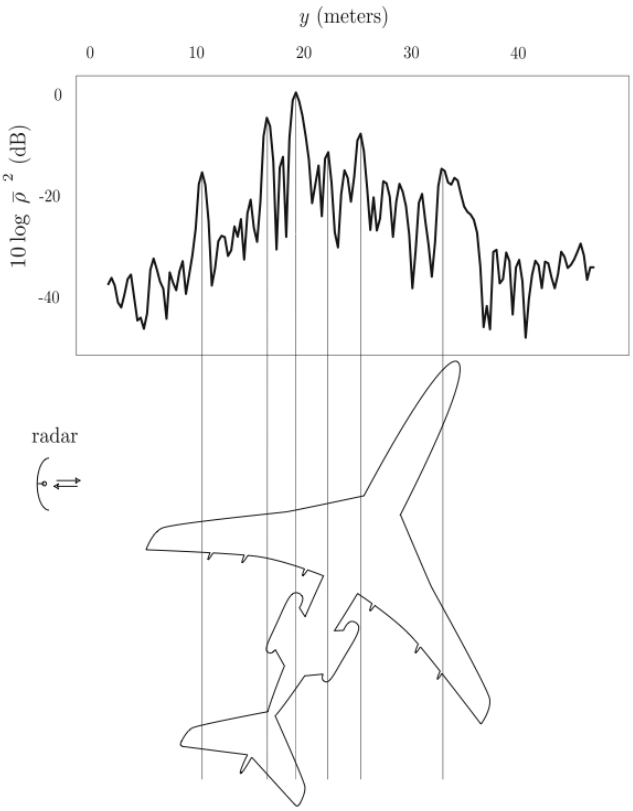

Figure 1. Example of a range profile from a B-727 jetliner. The top view (with orientation at time of measurement) is displayed beneath (From: [8])

The received signal of non-interacting, stationary targets can be expressed as

$$s_{rec}(t) = \int_{-\infty}^{\infty} \rho(\tau') s_{inc}(t-\tau') d\tau' + n(t) \tag{2.17}$$

where $n(t)$ is the random noise term. The correlation integral can be expressed as

$$\eta(\tau) = \int_{-\infty}^{\infty} s_{rec}(t')s_{inc}^{*}(t'-\tau)dt' = \int_{-\infty}^{\infty} s_{inc}^{*}(t'-\tau)\int_{-\infty}^{\infty} \rho(\tau')s_{inc}(t'-\tau')d\tau' dt' \quad + \quad \text{noise term}$$

$$\eta(\tau) = \iint_{-\infty}^{\infty} s_{inc}^{*}(t'-\tau)s_{inc}(t'-\tau')dt'\,\rho(\tau')d\tau' \quad + \quad \text{noise term} \tag{2.18}$$

Substituting $t'' = t'-\tau'$ and dropping the noise term gives

$$\eta(\tau) = \int_{-\infty}^{\infty} \chi(\tau-\tau')\rho(\tau')d\tau' \tag{2.19}$$

where χ is the autocorrelation function (in this case, it is also a point spread function.)

$$\chi(\tau) = \int_{-\infty}^{\infty} s^{*}(t''-\tau)s(t'')dt'' = \int_{-\infty}^{\infty} s^{*}(t')s(t'+\tau)dt' \tag{2.20}$$

The image is formed by the convolution of ρ and χ,

However, range profiles can be difficult to be used for target classification, since all scatterers located at the same distance from the radar will reflect the signal back with the same time-delay. As a result, the range profile will not be able to distinguish the cross range structure.

E. TWO-DIMENSIONAL IMAGING

A simple concept based on “triangulation” can be used to determine the cross-range target structure while still using an HRR radar system. Figure 2. illustrates this approach, which relies on range profiles collected from different target orientations and correlated to form a two-dimensional image.

Consider a set of three point targets with the radar located at the same distance from targets 2 and 3 in Figure 2. Given the orientation as shown, the return signal will only indicate two targets. Hence, ambiguity exists when targets are the same distance away from the radar.

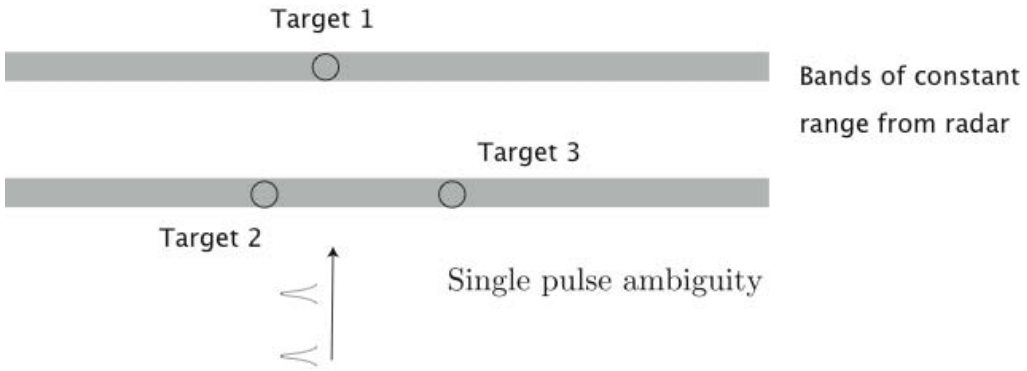

Figure 2. Ambiguous scenario from a single radar pulse (From: [6])

The return signals from multiple directions can be used to determine range and cross-range information. Hence, the range profiles are swept in the cross range direction to form bands representing possible locations of target scattering centers in space. The bands are then superimposed, and the crossing points are used to determine the scattering center locations.

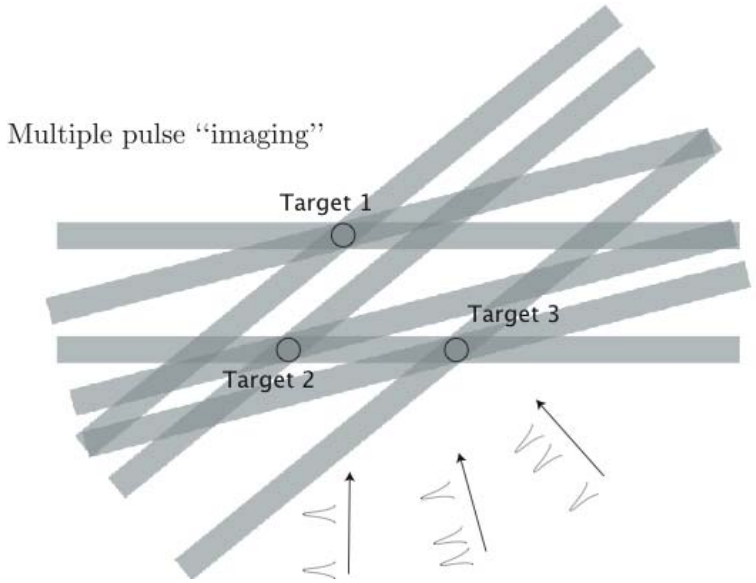

Figure 3. Cross-range information obtained from range profiles (From: [6])

There are 2 different schemes used to collect data from different target aspects. In one, the radar moves while the target remains stationary. This data collection process

occurs over a synthetic aperture and hence is called “synthetic aperture radar” (SAR). In the other, the target rotates while the radar is stationary and staring at the target. This data collection process is called “inverse synthetic aperture radar” (ISAR).

F. RADAR IMAGING—AN INVERSE PROBLEM

Normal radar can be approximated as a linear measurement system, which is also shift invariant. Radar imaging would not be possible if the time-delayed scattering signal looked different for different time delays. Hence, a radar imaging system can be expressed by the functional operator or “kernel” κ that describes how the measurement system works

$$m = \kappa f \tag{2.21}$$

Where m denotes the measurement at position x and f denotes the “object” function.

The direct problem in radar imaging refers to predicting the data measured by the radar from a known target. The inverse problem is the “reproduction” of the original unknown target from given radar measured data.

1. Well-Posed and Ill-Posed Problems

Radar systems, which are typically band-limited, do not allow a unique solution to the inverse problem. This is due to the fact they yield finite measurement data, which are noisy as well.

Using discrete measurement systems in which the measurement data are finite, Equation 2.16 can be written in matrix form. For such systems, the goal is to find a good estimate $\overline{f}$ of f from the measurements m which can be expressed symbolically as

$$\overline{f} = \kappa^{-1} m \tag{2.22}$$

The fact that the “kernel” κ is not always a square matrix poses some problems. In general, the matrix κ is N × M, and when $M > N$ there are more unknowns than there are linearly independent Equations and so the system cannot have a unique solution.

As the object space (M-dimensional) is larger than the measurement space (N-dimensional), a null space will exist, and it will consists of all vectors of the form $f - \kappa f$. The null space is determined by the kernel κ, which represents the measurement system. As such, the null space contains all things that cannot be measured. Null space accounts for image artifacts and must be carefully studied when interpreting reconstructed images.

In order to solve the inverse problem, it is often sufficient to search for approximate solutions satisfying additional constraints [9]. Since the set of approximate solutions is the set of objects with images closest to the measured one, $\overline{f}$ must obey

$$\kappa^T \kappa \overline{f} = \kappa^T m \tag{2.23}$$

This matrix Equation is also known as the "Normal Equation".

2. Data Reconstruction—Regularization

Equation (2.23) is the set of conditions that must be satisfied by the least-squares solution $\overline{f}$ which can be expressed as

$$\overline{f} = (\kappa^T \kappa)^{-1} \kappa^T m \tag{2.24}$$

Two techniques are commonly used, namely the singular value decomposition (SVD) and Tikhonov regularization. From linear algebra methods, the matrix $(\kappa^T \kappa)^{-1} \kappa^T$ can be expressed in terms of its SVD [6]:

$$(\kappa^T \kappa)^{-1} \kappa^T = UDV^T \tag{2.25}$$

where the matrices U and V contain the eigenvectors of $(\kappa^T \kappa)$, and D contains the reciprocal of the eigenvalues, which has diagonal elements of the form $1/\sqrt{\lambda_i}$ (where λ_i are the corresponding, non zero eigenvalues). Since κ is bounded, the eigenvalues must form a sequence that gets close to zero as the number of measurements (dimensions) increase, so their reciprocals become arbitrarily large. Since the data m are contaminated by noise, then the solution will multiply the noise by arbitrarily large values. Hence, the

simplest approach to mitigate the noise effect is to truncate the SVD representation and replace the component of D by zero if the corresponding eigenvalue falls below some threshold value. This method is called the truncation filter.

Tikhonov regularization makes an ad-hoc modification to the "Normal Equation" and can be rewritten as

$$\overline{f} = (\kappa^T \kappa + \alpha I)^{-1} \kappa^T m \tag{2.26}$$

Where α is a fixed scalar. When $\alpha = 0$, Equation (2.26) reverts to the "Normal Equation" and so it can be expected that small values of α will not change the system description significantly.

After introducing α, the diagonal elements of D in Equation (2.25) can be expressed as

$$D_{ii} = \frac{\sqrt{\lambda_i}}{\lambda_i + \alpha} \tag{2.27}$$

when $\lambda_i >> \alpha$, $D_{ii} \approx 1/\sqrt{\lambda_i}$ (as before). However, when $\lambda_i = \alpha$, $D_{ii} \approx \sqrt{\lambda_i} / \alpha$ and will not become arbitrarily large and the noise issue is moderated.

For limiting the effect of noise, both Truncation filters and Tikhonov regularization are powerful and useful methods. However, none offers a method to choose the "best" threshold value α. With too large α, the ability to accurately estimate the object will be affected, and too small α will not control the noise effectively.

THIS PAGE INTENTIONALLY LEFT BLANK

III. IMAGING AND THE MOVING TARGET DATA MODEL

The previous chapter discussed different types of imaging theories and techniques that are used for radar imaging. This chapter describes the ideas and concepts used to develop the imaging model for moving targets.

A. LINEARIZED DATA MODEL

The scattering model used to describe non moving targets is based on a scattered field using Born approximation and is

$$\Psi_{scatt}(x,t) = \iiint_D g(x',x;t',t)\rho(x')\psi_{inc}(x',t')d^3x' \tag{3.1}$$

where

$$g(x',x;t',t) = \frac{\delta(t-t'-|x'-x|/c)}{4\pi|x'-x|} \tag{3.2}$$

is the Green's function and, for a signal $s_y(t)$ transmitted from position y with starting time $-T_y$, it can be shown that the incident field at x is

$$\psi_{inc}(x,t) = -\frac{s_y(t+T_y-|x-y|/c)}{4\pi|x-y|} \tag{3.3}$$

The scattered field $\psi_{scatt}(y,z,t)$ at position z and time t is therefore

$$\psi_{scatt}(y,z,t) = \iint \frac{\delta(t-t'-|z-x'|/c)}{4\pi|z-x'|}\frac{s_y(t'+T_y-|x'-y|/c)}{4\pi|x'-y|}\rho(x')d^3x'dt' \tag{3.4}$$

By using the Born approximation and the time-domain Green function, we obtain the scattered field for non-moving scatterers as shown in Equation (3.4). However, we are generally interested in the scattered field from moving scatterers (targets), hence the scattering model shown in Equation (3.4) has to be modified.

The scattering density function $\rho(x)$ used in Equation (3.1) is only space dependent, since the target is not moving. It is like a scaling function, which attenuates the transmitted signal. For a moving target, the scattering density function is dependent on both distance and time, so it is expressed as $\rho(x,t)$.

So, we modify the scattering model by letting $\rho_v(x-vt)d^3xd^3v$ represent the scatterers in the volume element d^3xd^3v of phase space centered at position *x* and velocity *v*. Choose T_y to be the time of the transmitted signal such that the scattering density $\rho_v = \rho_v(x)$, which accounts for all targets that are moving with velocity *v* at time *t=0* (i.e., the time of the transmitted signal is activated at time $t=-T_y$). This shows that the spatial scatterer density centered at time *t* and position *x* is

$$\rho(x) = \int \rho_v(x-vt)d^3v \tag{3.5}$$

Hence, the scattered field is

$$\psi_{scatt}(y,z,t) = \iiint \frac{\delta(t-t'-|z-x'|/c)}{4\pi|z-x'|} \times \frac{s_y(t'+T_y-|x'-y|/c)}{4\pi|x'-y|}\rho_v(x'-vt')d^3vd^3x'dt' \tag{3.6}$$

By implementing the change of variables $x' \to x = x'-vt'$, the modified scattered field is

$$\psi_{scatt}(y,z,t) = \iiint \frac{\delta(t-t'-|x+vt'-z|/c)}{4\pi|x+vt'-z|} \times \frac{s_y(t'+T_y-|x+vt'-y|/c)}{4\pi|x+vt'-y|}\rho_v(x)d^3vd^3xdt' \tag{3.7}$$

Now, the scattered field of moving targets is incorporated into the data model. The physical interpretation of Equation (3.7) is that the electromagnetic wave generated from transmitter at position y at time $-T_y$ interacts with the target at time t'. During the interval $[0,t']$, the target has moved from position x to a new position $x+vt'$. The scattered field with strength $\rho_v(x)$ propagates from its new position $x+vt'$ to receiver at location z and at time t.

Equation (3.7) can be simplified, by letting

$$\boldsymbol{R}_{x,z}(t) = x + vt - z, \qquad R = |\,\boldsymbol{R}\,|, \qquad \hat{\boldsymbol{R}} = \boldsymbol{R} / R$$

and substituting into the scattered field Equation (3.6) we obtain

$$\psi_{scatt}(y,z,t) = \iiint \frac{\delta(t - t' - R_{x,z}(t')/c)}{4\pi R_{x,z}(t')} \times \frac{S_y(t' + T_y - R_{x,y}(t')/c)}{4\pi R_{x,y}(t')} \rho_v(x) d^3v d^3x dt' \qquad (3.8)$$

The dependence of $R_{x,z}(t')$ on the variable t' makes this integration complicated. To further simplify, we let $t' = \bar{t}_{x,v}(t)$, which denotes the implicit solution of

$$t - t' - R_{x,z}(t')/c = 0, \qquad \text{i.e.,} \quad t - \bar{t}_{x,v}(t) - R_{x,z}(\bar{t}_{x,v}(t))/c = 0$$

The integration over t' then yields

$$\psi_{scatt}(y,z,t) = \iint \frac{s_y\left(\bar{t}_{x,v}(t) + T_y - R_{x,y}(\bar{t}_{x,v}(t))/c\right)}{(4\pi)^2 R_{x,z}(\bar{t}_{x,v}(t)) R_{x,y}(\bar{t}_{x,v}(t))} \rho_v(x) d^3v d^3x \qquad (3.9)$$

By substituting $\bar{t}_{x,v}(t) = t - R_{x,z}(\bar{t}_{x,v}(t))/c$, we obtain

$$\psi_{scatt}(y,z,t) = \iint \frac{s_y\left(t + T_y - R_{x,z}(\bar{t}_{x,v}(t))/c - R_{x,y}(\bar{t}_{x,v}(t))/c\right)}{(4\pi)^2 R_{x,z}(\bar{t}_{x,v}(t)) R_{x,y}(\bar{t}_{x,v}(t))} \rho_v(x) d^3v d^3x \qquad (3.10)$$

B. FURTHER SIMPLIFYING APPROXIMATIONS

Equation (3.10) is applicable to most general scenarios. It is applicable to fast moving targets, where the start-stop approximation is not valid. It can also be used for any types of transmitted waveforms.

However, retarded-time problems are still present. These problems arise due to the definition of the retarded-time $\bar{t}_{x,v}(t)$. The retarded-time can be obtained by solving

$$\bar{t}_{x,v}(t) = t - R_{x,z}(\bar{t}_{x,v}(t))/c \qquad (3.11)$$

Hence, a more meaningful result can be obtained when the scatterers are moving in a known fashion so that $R_{x,z}(t)$ can be expanded in a Taylor series around $t = 0$ and approximated by retaining the terms linear in *t.* We refer to this approximation as "slow-moving" target.

1. The Slow-Mover Approximation

Assuming that $(|v|t)$ and $(|v|^2 t^2 \times \omega_{\max} / c)$ are much less than $|x - z|$ and $|x - y|$**,** where $\omega_{\max}$ denotes the maximum angular frequency of the transmitted signal s_y, we have

$$R_{x,z}(t) = |z - (x - vt)| = R_{x,z}(0) + \hat{\boldsymbol{R}}_{x,z}(0) \cdot vt + \ldots \tag{3.12}$$

where $\boldsymbol{R}_{x,z}(0) = \boldsymbol{x} - \boldsymbol{z}$, $R_{x,z}(0) = |\boldsymbol{R}_{x,z}(0)|$, and $\hat{\boldsymbol{R}}_{x,z}(0) = \boldsymbol{R}_{x,z}(0) / R_{x,z}(0)$. Substituting this result into the definition of retarded time yields,

$$\bar{t}_{x,v}(t) \approx t - \left(R_{x,z}(0) + \hat{\boldsymbol{R}}_{x,z}(0) \cdot \boldsymbol{v} \bar{t}_{x,\upsilon}(t) \right) / c \approx \frac{t - R_{x,z}(0)/c}{1 + \hat{\boldsymbol{R}}_{x,z}(0) \cdot \boldsymbol{v} / c} \tag{3.13}$$

Inserting this approximation into the result for $\psi_{scatt}(y,z,t)$ and simplifying yields

$$\psi_{scatt}(y,z,t) = \iint \frac{s_y\left(\alpha_{x,v}\left[t - R_{x,z}(0)/c\right] - R_{x,y}(0)/c + T_y\right)}{(4\pi)^2 R_{x,z}(0) R_{x,y}(0)} \rho_v(x) d^3v d^3x \tag{3.14}$$

where

$$\alpha_{x,v} \equiv \frac{1 - \hat{R}_{x,y}(0) \cdot v / c}{1 + \hat{R}_{x,z}(0) \cdot v / c} \tag{3.15}$$

$\alpha_{x,v}$ is the Doppler scale factor.

2. The Slow-Mover and Narrow-Band Approximation

Radar systems are typically narrow-band, and the transmitted signal is usually of the form

$$s_y(t) = \tilde{s}_y(t)e^{-i\omega_y t} \tag{3.16}$$

where $\tilde{S}_y(t)$ is slowly varying when compared to $e^{-i\omega_y t}$, with ω_y the carrier frequency of the transmitter y. The second time derivatives of $s_y(t)$ are dominated by the $e^{-i\omega_y t}$ factor, and by implementing the slowly varying and narrow-band approximation, we obtain,

$$\begin{aligned}\psi_{scatt}(y,z,t) &= -\iint \frac{\omega_y^2 e^{i\varphi_{x,v}} e^{-i\omega_y \alpha_{x,v} t}}{(4\pi)^2 R_{x,z}(0)R_{x,y}(0)} \\ &\times \tilde{s}_y\left(t + T_y - (R_{x,z}(0) + R_{x,y}(0))/c\right)\rho_v(x)d^3v d^3x\end{aligned} \tag{3.17}$$

where

$$\varphi_{x,v} \equiv \omega_y^2\left[R_{x,y}(0) - cT_y + \alpha_{x,v}R_{x,z}(0)\right]/c \tag{3.18}$$

3. The Slow-Mover, Narrow-Band and Far-Field Approximation

When the distances from the transmitter to target and target to the receiver are large in comparison with the imaging scene dimensions, then $|x + vt|$ and $|x + vt|^2 \times \omega_{\max}/c$ can be assumed to be much less than either $|z|$ or $|y|$. Therefore, the expansion

$$R_{x,z}(t) = |z - (x - vt)| = |z| - \hat{z}\cdot(x + vt) + \ldots$$

can be applied (and similarly for $R_{x,y}(t)$). Substituting the expansions into previous approximations Equation (3.17) then yields

$$\psi_{scatt}(y,z,t) \approx \frac{-\omega_y^2}{(4\pi)^2 \mid z \mid \mid y \mid} \iint e^{i\varphi_{x,v}} e^{-i\omega_y \alpha_{x,v} t} \times \tilde{s}_y \left(t + T_y - (\mid z \mid - \hat{z} \cdot \boldsymbol{x} + \mid y \mid - \hat{y} \cdot \boldsymbol{x}) / c \right) \rho_v(x) d^3 v d^3 x \tag{3.19}$$

where

$$\varphi_{x,v} \equiv \omega_y \left[\mid y \mid - \hat{y} \cdot \boldsymbol{x} - cT_y + \alpha_v (\mid z \mid - \hat{z} \cdot \boldsymbol{x}) \right] / c \tag{3.20}$$

The Doppler scale factor can also be approximated as

$$\alpha_\upsilon \approx \frac{1 - \hat{y} \cdot \boldsymbol{v} / c}{1 + \hat{z} \cdot \boldsymbol{v} / c} \approx 1 - (\hat{y} + \hat{z}) \cdot \boldsymbol{v} / c \tag{3.21}$$

because $| \boldsymbol{v} | / c << 1$. The quantity $\omega_y \times \beta_v$ is the Doppler shift (where $\beta_v \equiv -(\hat{y} + \hat{z}) \cdot \boldsymbol{v} / c$)

By inserting $T_y = | y | / c$ and $k_y \equiv \omega_y / c$ we obtain

$$\varphi_{x,v} \equiv k_y \mid \boldsymbol{z} \mid - k_y (\hat{y} + \hat{z}) \cdot \left[\boldsymbol{x} + (\hat{z} \cdot (\boldsymbol{z} - \boldsymbol{x})) \boldsymbol{v} / c \right] \tag{3.22}$$

C. IMAGING VIA A FILTERED ADJOINT

In developing the correlation receiver, it is observed that how much two signal functions (complex-valued) look alike is given by the cross correlation. The correlation integral measures how much the received signal "looks like" the time-delayed, frequency-shifted version of the transmitted signal. A large value of the correlation integral indicates a strong resemblance, while a small value indicates a weak resemblance.

Using the same notion, the usual radar model is developed for the scattered field of a point target, which is a time-delayed and Doppler shifted version of the incident field. This two-parameter model is a cross correlation between the received signal and the transmitted signal. The values of the time-delayed and Doppler shift parameters, which maximize the cross-correlation, are the parameters that most represent the target.

The generalized model for $\psi_{scatt}(y,z,t)$ depends on the position of the scatterer $\boldsymbol{x}=(x_1,x_2,x_3)$ and its velocity $\boldsymbol{v}=(v_1,v_2,v_3)$. Using $\psi_{scatt}(y,z,t)$ to build a six-parameter scattering model based on the arbitrary position $\boldsymbol{p}=(p_1,p_2,p_3)$ and arbitrary velocity $\boldsymbol{u}=(u_1,u_2,u_3)$ of any scatterer, the values of $\boldsymbol{p}$ and $\boldsymbol{u}$ that maximize the cross correlation between the arbitrary model and the measured data will represent the "best fit" of $\boldsymbol{p}$ and $\boldsymbol{u}$ to the data. These values of $\boldsymbol{p}$ and $\boldsymbol{u}$ will localize the position and velocity of any unknown scatterers in the position-velocity space (phase space).

The scattered field from known scatterers $\rho_v(x)$ with positions *x* and velocities *v* is

$$\psi_{scatt}(y,z,t)\approx\frac{-\omega_y^2 e^{-i\omega_y(t-|z|/c)}}{(4\pi)^2\,|\,z\,||\,y\,|}\iint\exp\left\{-ik_y(\hat{y}+\hat{z})\cdot[x-v(t-z\cdot(z-x)/c)]\right\}\times\tilde{s}_y\left(t-(|\,z\,|-(\hat{y}+\hat{z})\cdot x)/c\right)\rho_v(x)d^3vd^3x \tag{3.23}$$

To simplify, substitute $t'=t-|\,z\,|/c$,

$$\psi_{scatt}(y,z,t')\approx\frac{-\omega_y^2 e^{-i\omega_y t'}}{(4\pi)^2\,|\,z\,||\,y\,|}\iint\exp\left\{-ik_y(\hat{y}+\hat{z})\cdot[x-v(t'+\hat{z}\cdot x/c)]\right\}\times\tilde{s}_y\left(t'+(\hat{y}+\hat{z})\cdot x/c\right)\rho_v(x)d^3vd^3x \tag{3.24}$$

By ignoring the intensity prefactor, a parametric model representing the field from an unknown point source is

$$\psi(y,z,t')=-e^{-i\omega_y t'}\exp\left\{-ik_y(\hat{y}+\hat{z})\cdot[p-u(t'+\hat{z}\cdot p/c)]\right\}\times\tilde{s}_y\left(t'+(\hat{y}+\hat{z})\cdot p/c\right) \tag{3.25}$$

Based on the cross-correlation notion, an image can be created as follows:

$$I(p,u)=\iiint\psi_{scatt}(y,z,t')\psi^*(y,z,t')dt'd^m yd^n z \tag{3.26}$$

where m, n depends on the number of the transmitter(s)/receiver(s), and the integrals are over all values of t', y and z for which data are measured. Large values of $|I(p,u)|$ indicate a strong resemblance while low values of $|I(p,u)|$indicate a mismatch. True cross correlation will not be possible if the data measured is not for all t', y and z, therefore the best approximation to cross correlation with limited data will result in image artifacts. Due to these artifacts, a filter function $Q(\omega,t',p,u,y,z)$ is included to suppress those artifacts,

$$I(p,u)=\iiint \psi_{scatt}(y,z,t')\psi^{*}(y,z,t')Q(\omega,t',p,u,y,z)dt'd^{m}yd^{n}z \tag{3.27}$$

Hence, the image is formed as,

$$\begin{aligned} I(p,u)=&-\iiint Q(\omega,t',p,u,y,z)e^{i\omega_y t'}e^{ik_y(\hat{y}+\hat{z})\cdot\left[p-u(t'+\hat{z}\cdot p/c)\right]} \\ &\times\tilde{s}_y^{*}\left(t'+(\hat{y}+\hat{z})\cdot p/c\right)\psi_{scatt}(y,z,t')dt'd^{m}yd^{n}z \end{aligned} \tag{3.28}$$

D. IMAGE ANALYSIS

To determine the effectiveness of this imaging model, we work various scenarios. By inserting the ideal measured data back into the imaging Equation (3.28) and substituting $\psi_{scatt}(y,z,t')$ we obtain,

$$\begin{aligned} I(p,u)=&\iiint\iint\frac{\omega_y^2 Q(\omega,t',p,u,y,z)}{(4\pi)^2|z||y|}\rho_v(x) \\ &\times\exp\left\{ik_y(\hat{y}+\hat{z})\cdot[p-x-(u-v)t'-u(\hat{z}\cdot p)/c+v(\hat{z}\cdot x)/c]\right\} \\ &\times\tilde{s}_y^{*}\left(t'+(\hat{y}+\hat{z})\cdot p/c\right)\tilde{s}_y\left(t'+(\hat{y}+\hat{z})\cdot x/c\right)d^3vd^3xdt'd^{m}yd^{n}z \end{aligned} \tag{3.29}$$

The distances $|z|$ and $|y|$ are amplitude scaling factors and not important for imaging purposes. Thus we can choose

$$Q(\omega,t',p,u,y,z)=\frac{(4\pi)^2|z||y|}{\omega_y^2}J(p,u,y,z) \tag{3.30}$$

where $J(p,u,y,z)$ is geometry dependent and is used to compensate for the Jacobian that results,

$$\begin{aligned} I(p,u) = \iiiint \tilde{s}_y^*\left(t'+(\hat{y}+\hat{z})\cdot p/c\right)\tilde{s}_y\left(t'+(\hat{y}+\hat{z})\cdot x/c\right)e^{-ik_y(\hat{y}+\hat{z})\cdot(u-v)t'} \\ \times\exp\left\{ik_y(\hat{y}+\hat{z})\cdot[p-x-u(\hat{z}\cdot p)/c+v(\hat{z}\cdot x)/c]\right\} \\ \times J(p,u,y,z)\rho_v(x)dt'd^3vd^3xd^my d^nz \end{aligned} \tag{3.31}$$

This result can be written as

$$I(p,u) = \iint K(p,u,y,z)\rho_v(x)d^3vd^3x \tag{3.32}$$

where

$$\begin{aligned} K(p,u,y,z) = \iint \exp\left\{-ik_y(\hat{y}+\hat{z})\cdot[u(\hat{z}\cdot p)-v(\hat{z}\cdot x)]/c\right\} \\ \times\int \tilde{s}_y^*\left(t'+(\hat{y}+\hat{z})\cdot p/c\right)\tilde{s}_y\left(t'+(\hat{y}+\hat{z})\cdot x/c\right)e^{-ik_y(\hat{y}+\hat{z})\cdot(u-v)t'}dt' \\ \times J(p,u,y,z)d^my d^nz \end{aligned} \tag{3.33}$$

is the point-spread function describing the behavior of the imaging system. By applying the change of variables $t = t'+\frac{1}{2}(\hat{y}+\hat{z})\cdot(p+x)/c$ and set $\tau \equiv (\hat{y}+\hat{z})\cdot(p-x)/c$ we obtain,

$$\begin{aligned} K(p,u,y,z) = \iint \exp\left\{-ik_y(\hat{y}+\hat{z})\cdot[u(\hat{z}\cdot p)-v(\hat{z}\cdot x)]/c\right\} \\ \times\exp\left\{ik_y(\hat{y}+\hat{z})\cdot[(p-x)+\frac{1}{2}(u-v)(\hat{y}+\hat{z})\cdot(p+x)]/c\right\} \\ \times\left[\int_{-\infty}^{\infty}\tilde{s}_y^*\left(t+\frac{1}{2}\tau\right)\tilde{S}_y\left(t-\frac{1}{2}\tau\right)e^{-ik_y(\hat{y}+\hat{z})\cdot(u-v)t}dt\right]J(p,u,y,z)d^my d^nz \end{aligned} \tag{3.34}$$

The integral in square brackets is the radar ambiguity function

$$\chi(\upsilon,\tau) = \int_{-\infty}^{\infty}\tilde{s}_y^*\left(t+\frac{1}{2}\tau\right)\tilde{s}_y\left(t-\frac{1}{2}\tau\right)e^{-i\upsilon t}dt$$

Hence, the imaging PSF can be written as

$$K(p,u,y,z) = \iint \exp\left\{-ik_y(\hat{y}+\hat{z})\cdot[u(\hat{y}\cdot p)-v(\hat{z}\cdot x)]/c\right\}$$
$$\times \exp\left\{ik_y(\hat{y}+\hat{z})\cdot[(p-x)+\frac{1}{2}(u-v)(\hat{y}+\hat{z})\cdot(p+x)]/c\right\} \quad (3.35)$$
$$\times \chi\left(k_y(\hat{y}+\hat{z})\cdot(u-v),(\hat{y}+\hat{z})\cdot(p-x)/c\right) J(p,u,y,z)d^m y d^n z$$

The point spread function, $K(p,u,y,z)$, depends on the geometry of the transmitter and receivers and also on the transmitting waveform used. When it is shift invariant, it can be used to determine the position and velocity resolution of the imaging scene for a given imaging configuration. By examining K, one can effectively model the image scene with meaningful resolution.

IV. RESULTS AND CONCLUSION

This chapter describes how the imaging model developed in Chapter III is implemented and analyzed. Using the same notion described in Chapter III, three sets of MATLAB programs were developed for the analysis. In this thesis, a four-parameter imaging model is considered, using the two-dimensions of position $\boldsymbol{x} = (x_1, x_2)$ and two-dimensions of velocity $\boldsymbol{v} = (v_1, v_2)$.

A. MODELS

1. The Scattering Model

The scattering model $\psi_{scatt}(y,z,t)$, as described in Equation (3.19), is basically a representation of the measured data from any scatterers. It contains information of the position $\boldsymbol{x} = (x_1, x_2)$ and velocity $\boldsymbol{v} = (v_1, v_2)$ of the unknown scatterers. A MATLAB code was built based on a four-parameter scattering model and different types of waveforms.

2. The Resolution Model

The point spread function, $K(p,u,y,z)$, as described in Equation (3.35), basically defines the resolution of the imaging scene. It depends on the geometry of the transmitters and receivers location and also on the types of waveforms used. Modifications were made to the codes developed by previous theses [10,11] to cater to a larger number of transmitters and receivers.

3. The Imaging Model

The imaging model, as described in Equation (3.28), is the main focus of this thesis. The imaging model uses the cross correlation between the expected target position and velocity with the scattering model to localize the position and velocity of the scatterer.

The focus of this thesis is the imaging of point targets. The imaging model in Equation (3.28) is not restricted to any type of transmitted waveform and is independent of the geometry of the transmitter/receiver configuration. The objective of this thesis is to study the behavior of this new imaging model with single pulse waveforms in different transmitter/receiver configurations.

Two configurations are considered. The transmitter/receivers geometries used for the simulation are shown in Figure 4(a) and 4(b). The receivers are denoted by "Δ", while the transmitter is denoted by "$\times$". Figure 4(a) shows the geometry of the linear array of receivers, while Figure 4(b) shows the geometry of the circular array of receivers.

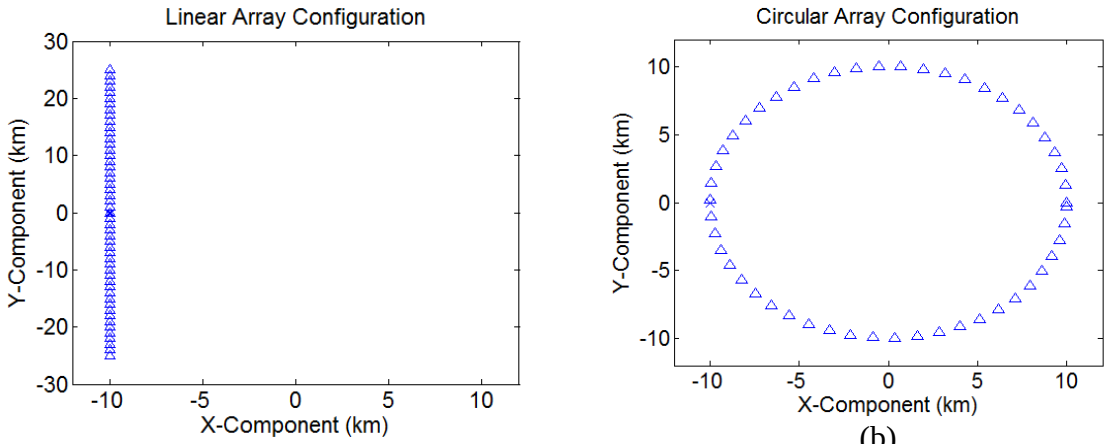

Figure 4. Geometry of The Transmitter and Receivers in (a) Linear Array Configuration and (b) Circular Array Configuration

B. THE SCATTERING MODEL

Assuming the simplest case, in which there is one transmitter and one receiver, both located at same position, 10 km away from the origin (-10km, 0), we consider three targets located at (-1000, 0), (-200,0), and (400,0) respectively. The scattering data from the three targets are shown in Figure 5.

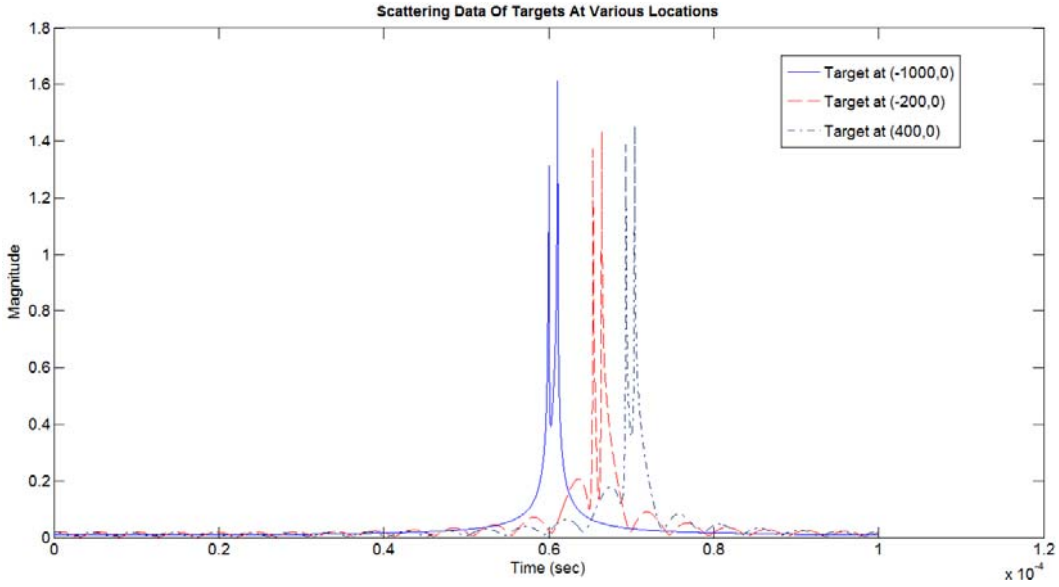

Figure 5. Scattering Data from Targets At Various Locations

From the scattering data shown in Figure 5. , it is observed that the scattering signal is a time-delayed version of the transmitted pulse. The further away the target is from the transmitter and receiver, the greater the time delay.

Figure 6. shows the scattering data from these targets using the linear array configuration, and Figure 6. shows the scattering data from the targets using the circular array configuration.

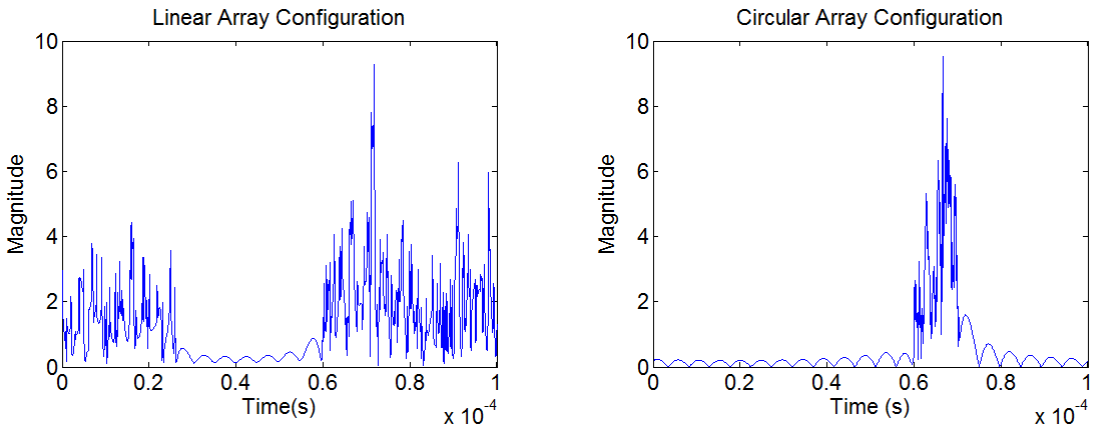

(a) (b)

Figure 6. Scattering Data From Targets At Various Locations

C. THE RESOLUTION MODEL

The position and velocity resolutions of the image are determined by their point spread function, which depends on the pulse width and the transmitter and receiver geometries. In order to analyze how various waveforms and geometries affect the resolution of the imaging system, two simple waveforms were selected: namely a single rectangular pulse and a single chirp pulse. The geometries used were the linear array and circular array configuration shown in Figure 4. .

1. Single Rectangular Pulse

Using a single rectangular pulse of width of 1 micro second as the transmitted waveform, the -3 dB position resolution obtained for the linear array configuration and circular array configuration is shown in Figure 7. . The -3 dB velocity resolution obtained for the linear array configuration and circular array configuration is shown in Figure 8. .

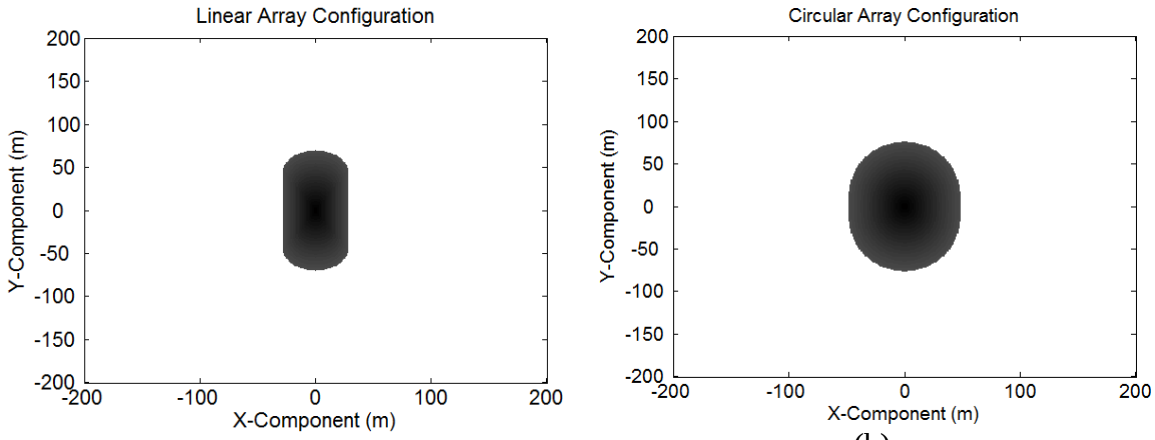

(a) (b)

Figure 7. The -3 dB position resolution of 1 μs rectangular pulse for (a) linear array configuration and (b) circular array configuration

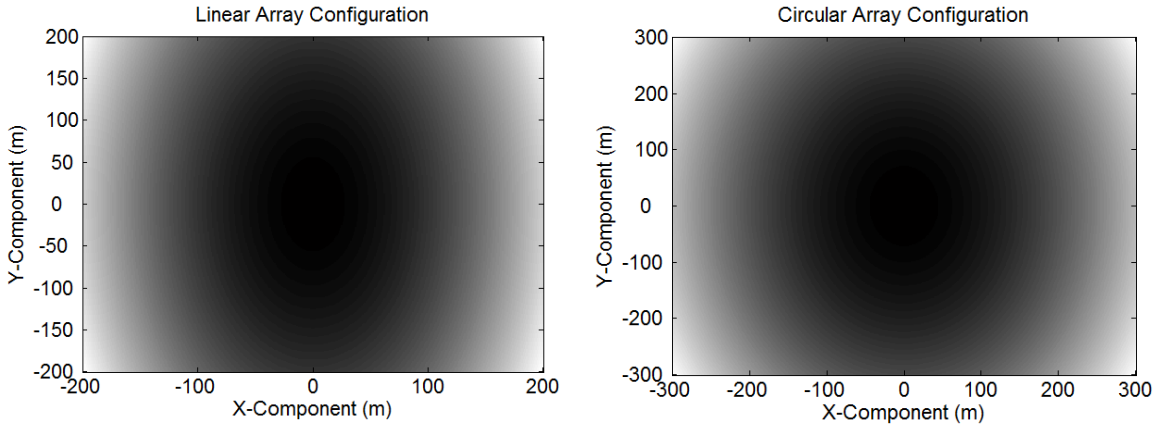

(a) (b)

Figure 8. The -3 dB velocity resolution of 1 μs rectangular pulse for (a) linear array configuration and (b) circular array configuration

The linear array configuration has a position resolution that is narrower in the x-components and broader in the y-components, while the position resolution has a more uniform resolution in both the x-components and y components. However, both configurations have very poor velocity resolution (which is not meaningful for spatial imaging purposes).

By using a longer rectangular pulse with pulse-width of 50 micro seconds as the transmitted waveform, the $-3\,\mathrm{dB}$ position resolution obtained for the linear array configuration and circular array configuration is shown in Figure 9. . The $-3\,\mathrm{dB}$ velocity resolution obtained for the linear array configuration and circular array configuration is shown in Figure 8. .

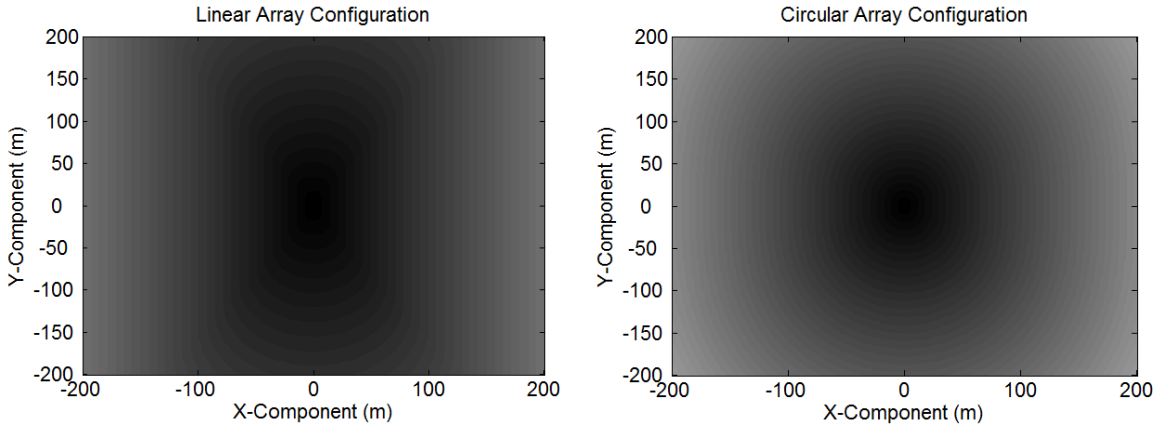

(a) (b)

Figure 9. The $-3\,\mathrm{dB}$ position resolution of 50 μs rectangular pulse for (a) linear array configuration and (b) circular array configuration

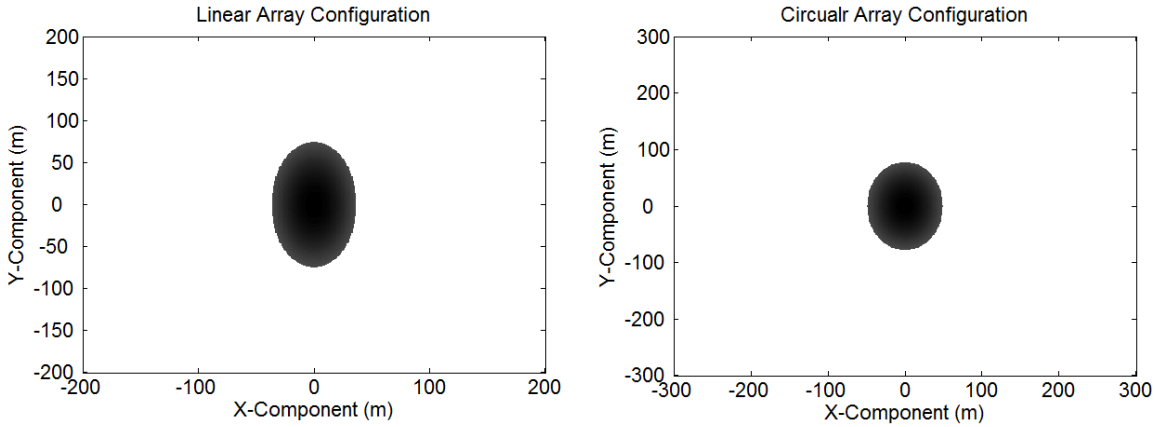

(a) (b)

Figure 10. The $-3\,\mathrm{dB}$ velocity resolution of 50 μs rectangular pulse for (a) linear array configuration and (b) circular array configuration

As shown in Figure 9. , both configurations have poor position resolution. However, as shown in Figure 10. the velocity resolution has improved.

These examples show that a smaller pulse-width has good position resolution, while a broader pulse-width has good velocity resolution. The geometry does affect the x and y components of the both the velocity and position resolution.

2. Single Chirp Pulse

A single chirp pulse with a one micro second pulse-width having a chirp rate of 0.5×10^{12} Hz/s is used as the transmitted waveform. The -3 dB position resolution obtained for the linear array and circular array is shown in Figures 11 The -3 dB velocity resolution obtained for the linear array and circular array is shown in Figure 12.

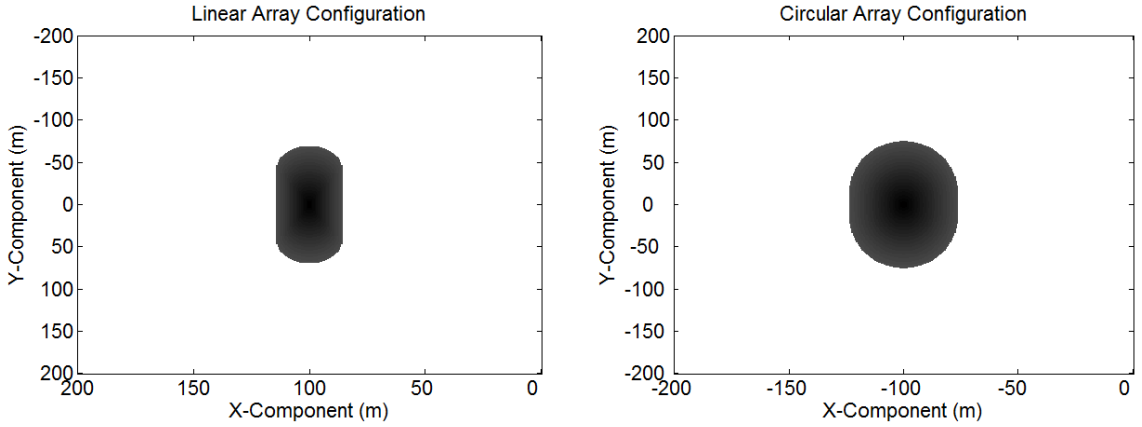

(a) (b)

Figure 11. The -3 dB position resolution of 1 μs pulse with chirp rate of 0.5×10^{12} Hz/s for (a) linear array configuration and (b) circular array configuration

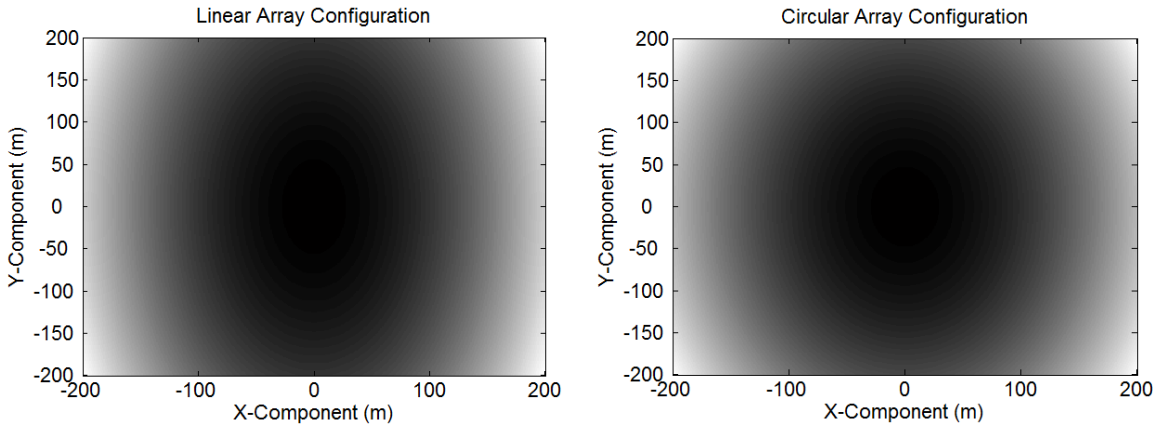

(a) (b)

Figure 12. The -3 dB velocity resolution of 1 μs pulse with chirp rate of 0.5×10^{12} Hz/s for (a) linear array configuration and (b) circular array configuration

From Figures 11 and 12, it is observed that the position and the velocity resolution is the same as the rectangular pulse of 1 micro second width. Where there is good position resolution and poor velocity resolution.

Figures 13 and 14 show the position and velocity resolution of a higher chirp rate. Using a higher chirp rate of 10×10^{12} Hz/s, the position resolution has improved significantly. However, the velocity resolution is still poor.

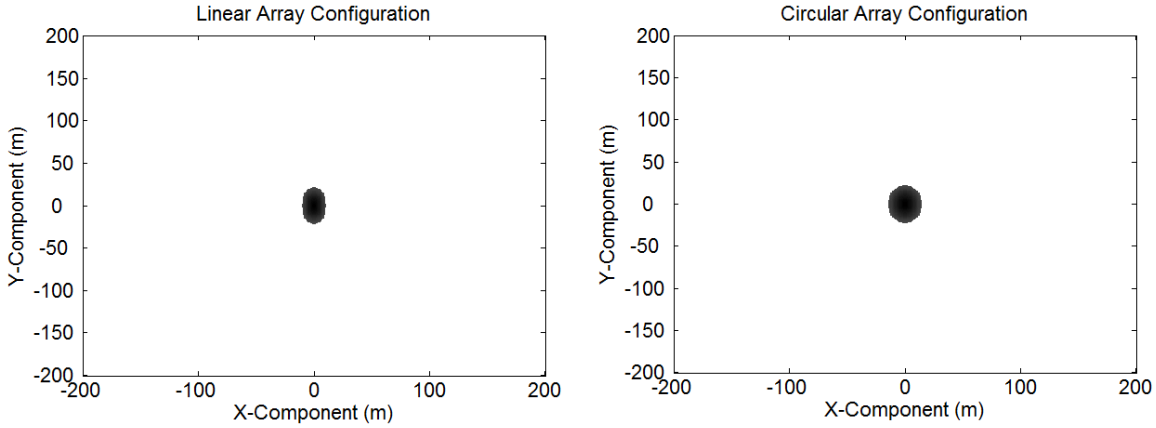

(a) (b)

Figure 13. The -3 dB position resolution of 1 μs pulse with chirp rate of 10×10^{12} Hz/s for (a) linear array configuration and (b) circular array configuration

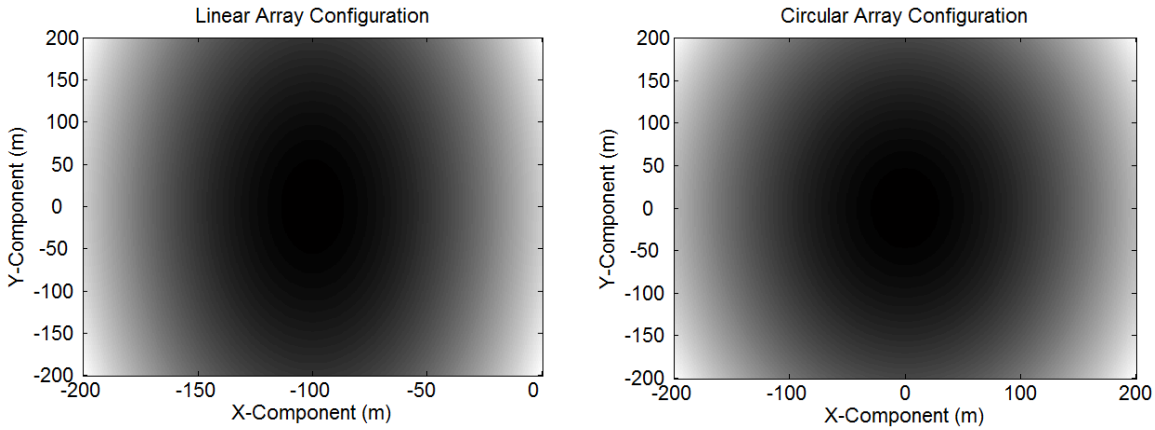

(a) (b)

Figure 14. The -3 dB velocity resolution of 1 μs pulse with chirp rate of 10×10^{12} Hz/s for (a) linear array configuration and (b) circular array configuration

A broader pulse width is used to analyze the effects of both the position and velocity resolution. Using a fifty micro second pulse width and a chirp rate of 0.5×10^{12} Hz/s, the results are shown in Figures 15 and 16.

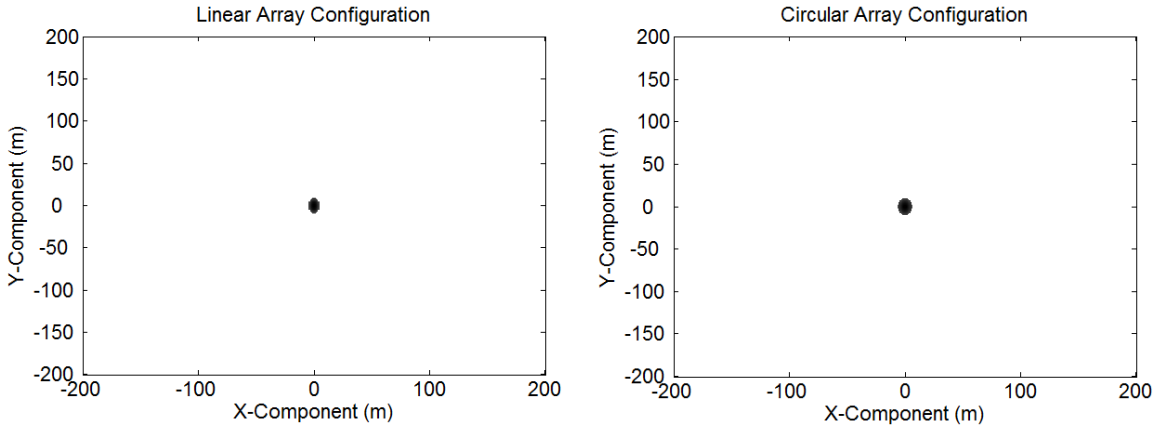

(a) (b)

Figure 15. The -3 dB position resolution of 50 μs pulse with chirp rate of 0.5×10^{12} Hz/s (a) linear array configuration and (b) circular array configuration

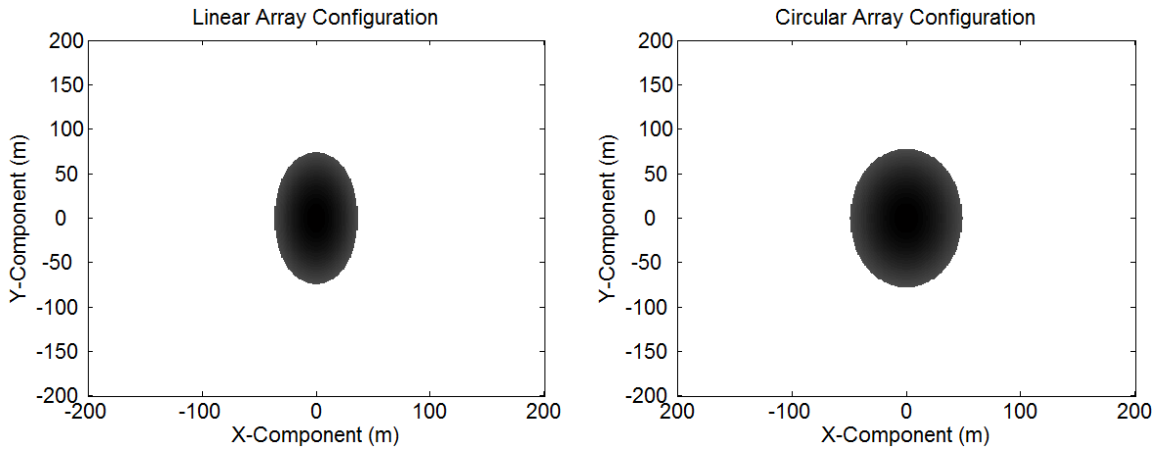

(a) (b)

Figure 16. The -3 dB velocity resolution of 50 μs pulse with chirp rate of 0.5×10^{12} Hz/s for (a) linear array configuration and (b) circular array configuration

From Figures 15 and 16, it is observed that the position and velocity resolutions have improved. Figures 17 and 18 shows the results of a $50\mu s$ pulse width and a chirp rate of 10×10^{12} Hz/s.

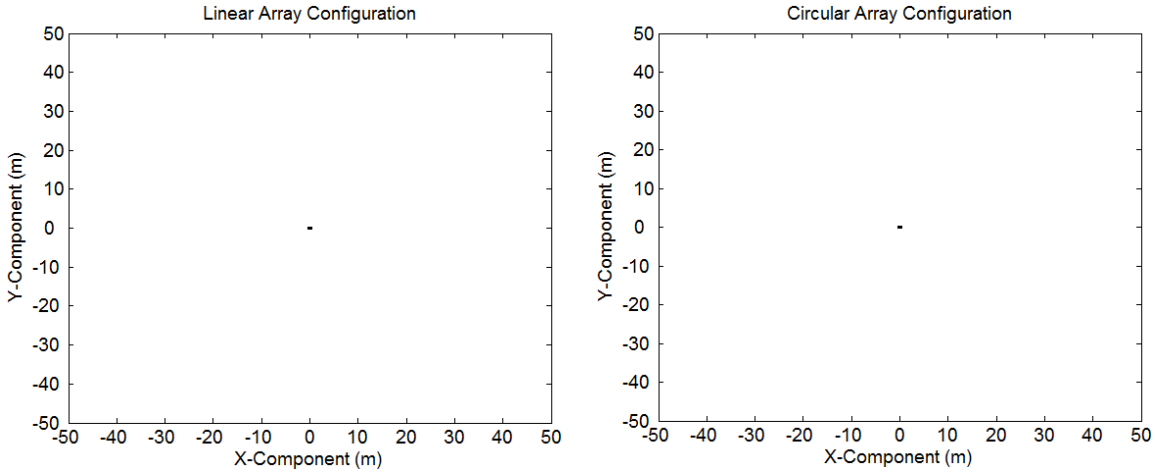

(a) (b)

Figure 17. The -3 dB position resolution of 50 μs pulse with chirp rate of 10×10^{12} Hz/s for (a) linear array configuration and (b) circular array configuration

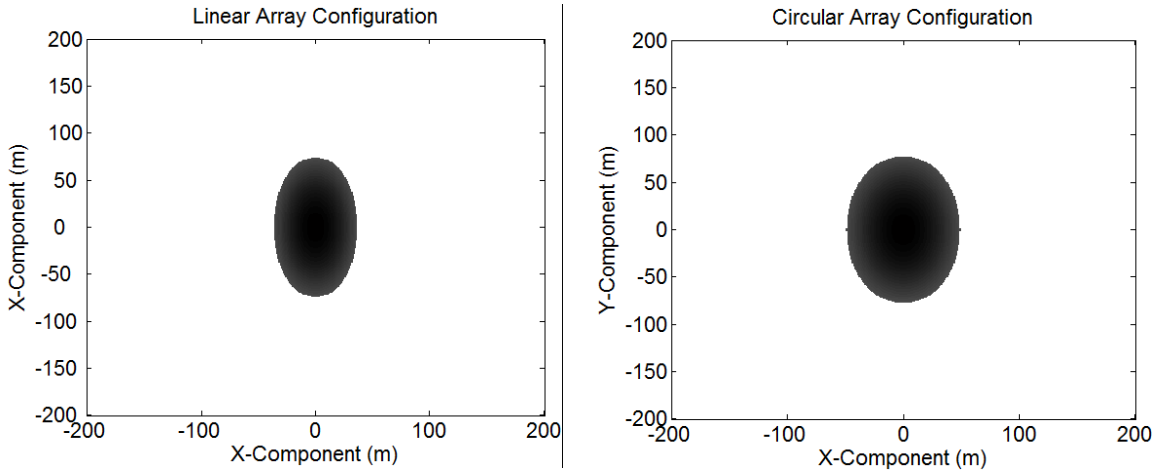

(a) (b)

Figure 18. The -3 dB velocity resolution of 50 μs pulse with chirp rate of 10×10^{12} Hz/s for (a) linear array configuration and (b) circular array configuration

From Figure 17, it is clearly seen that the position resolution is very fine, which is good for localizing targets, however Figure 18 shows no improvement in the velocity resolution.

From the chirp pulse analysis, it is observed that velocity resolution depends on the length of the pulse-width: the broader the pulse, the finer the velocity resolution. The position resolution depends on the chirp rate, the higher the chirp rate, the finer the position resolution. Waveform selection is important for imaging moving targets; it must have the ability to resolve the target's position and velocity of interest.

D. THE IMAGING MODEL

Three targets are used to analyze the behavior of the imaging model. The targets position x and velocity v are $x_1(-35,25)$, $x_2(-20,-30)$, $x_3(-40,45)$, and $v_1(0,-5)$, $v_2(10,10)$, $v_3(-5,-10)$ The transmitter and receiver geometries are the linear array configuration and circular array configuration as described earlier.

1. Linear Array Configuration

Figures 19, 20, and 21 show the image output based on the expected velocity $u_1(0,-5)$, $u_2(10,10)$ and $u_3(-5,-10)$ respectively.

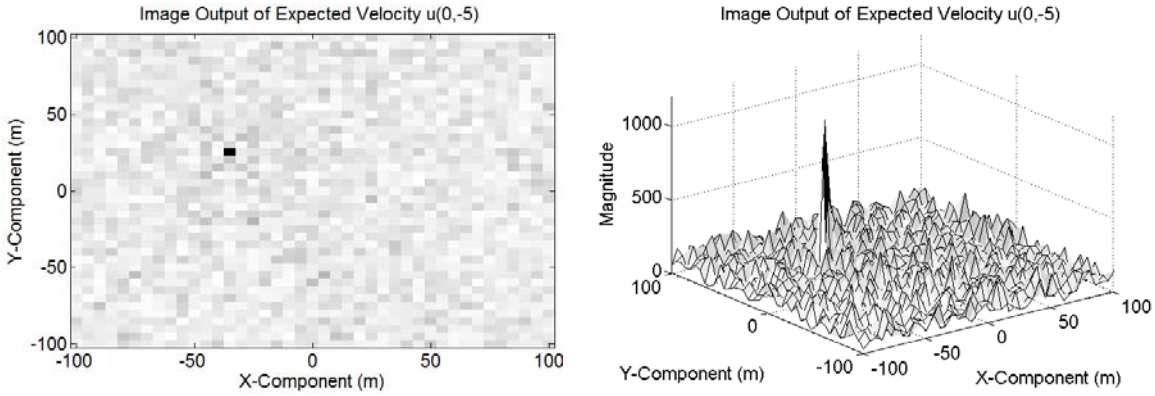

Figure 19. Image output of expected velocity of $u_1(0,-5)$

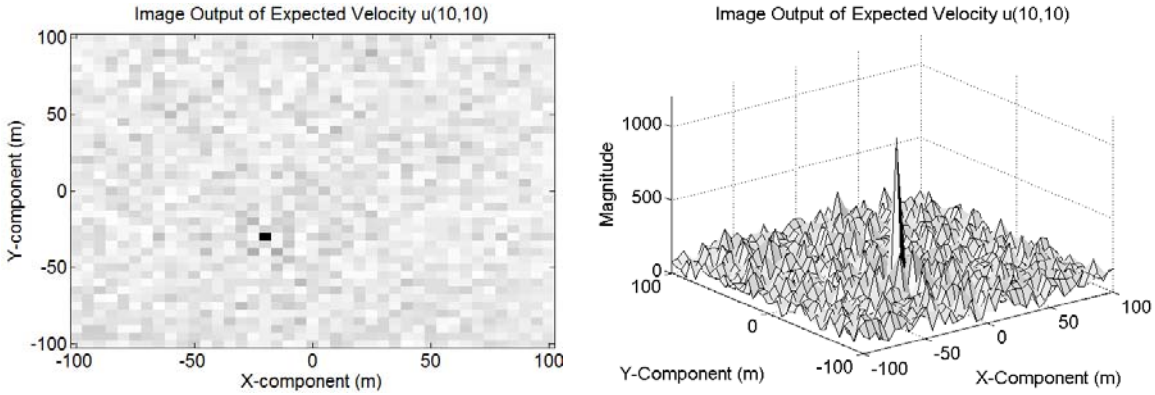

Figure 20. Image output of expected velocity of $u_2(10,10)$

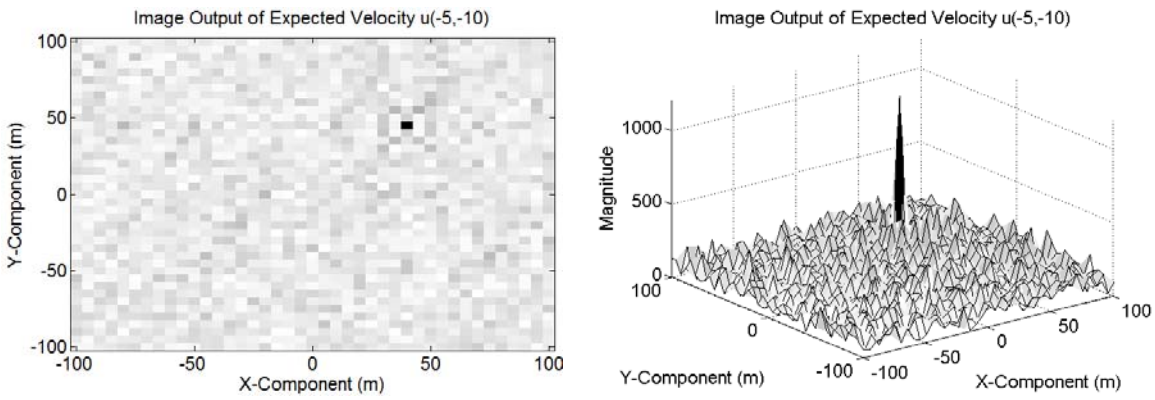

Figure 21. Image output of expected velocity of $u_3(-5,-10)$

All the images output show that the target positions are localized accurately without significant artifacts. A threshold level of 3dB lower than the peak is used to reject the image artifacts. Figure 22 shows the image output after the threshold is applied

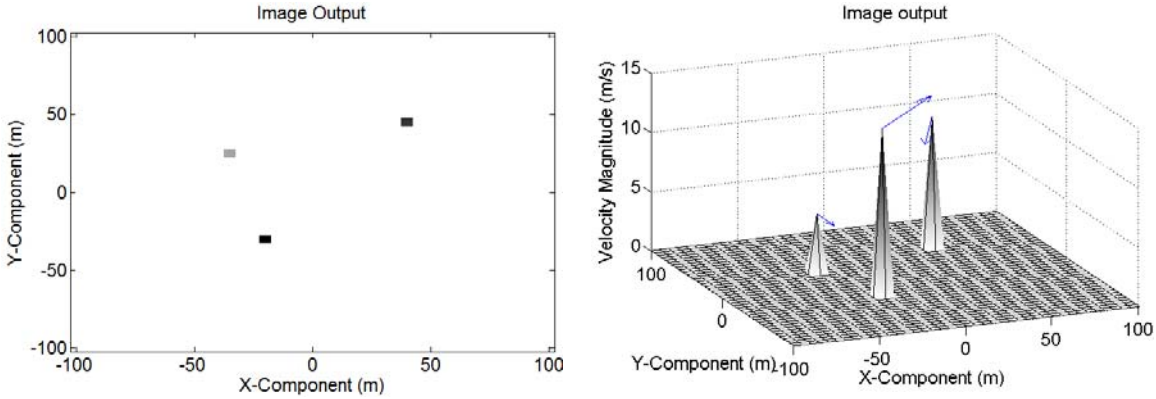

Figure 22. Threshold image output of all expected velocity space

Figure 22. shows a very clean image output with corresponding velocity vectors assigned. This is achievable mainly due to the cross correlation value of the artifacts, which are small compared to the cross correlation values that are “matched”.

2. Circular Array Configuration

Figures 23, 24, and 25 show the image output based on the expected velocity, $u_1(0,-5)$, $u_2(10,10)$ and $u_3(-5,-10)$ respectively

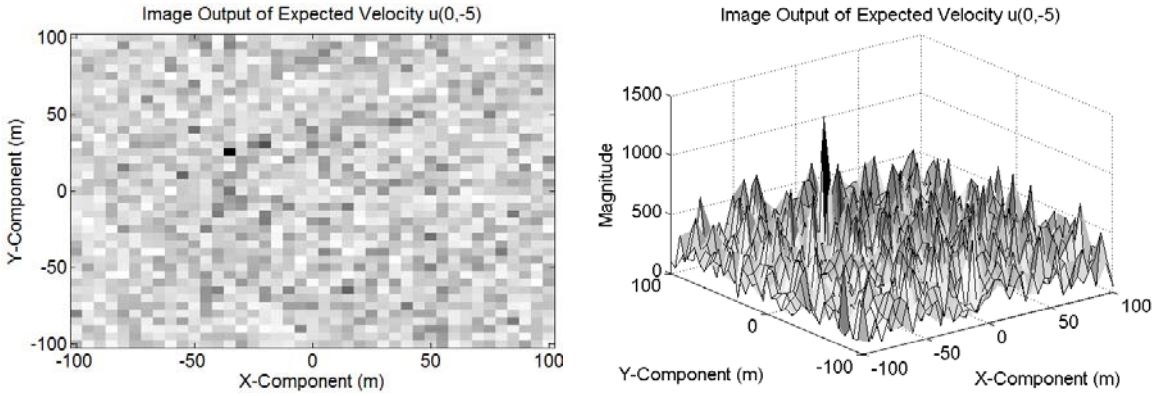

Figure 23. Image output of expected velocity of $u_1(0,-5)$

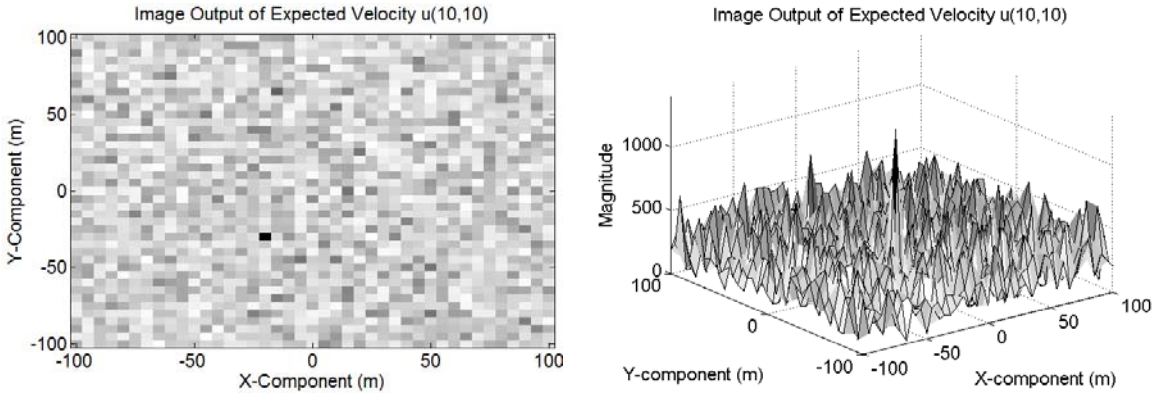

Figure 24. Image output of expected velocity of $u_2(10,10)$

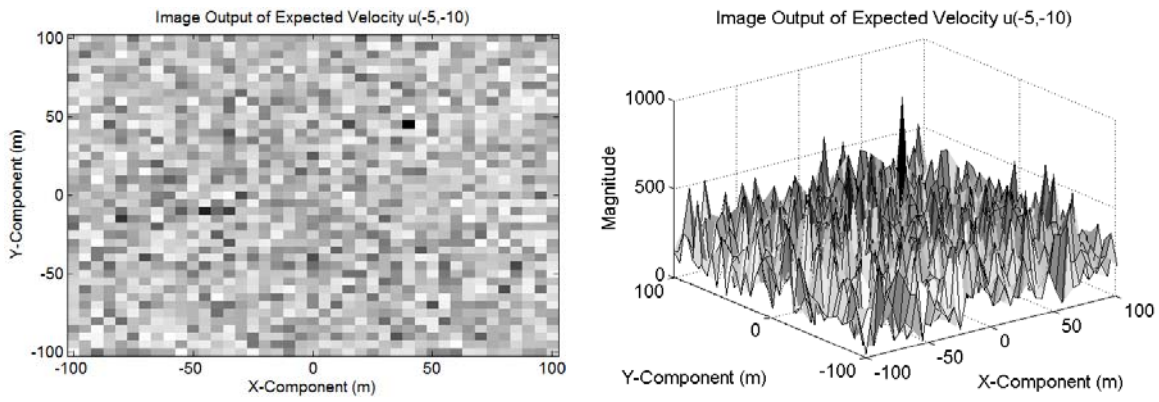

Figure 25. Image output of expected velocity of $u_3(-5,-10)$

All the images show that the target positions are localized accurately; however, in this configuration there are more image artifacts. A threshold level of 3dB lower than the peak is used to reject the image artifacts. Figure 26 shows the image output after the threshold is applied

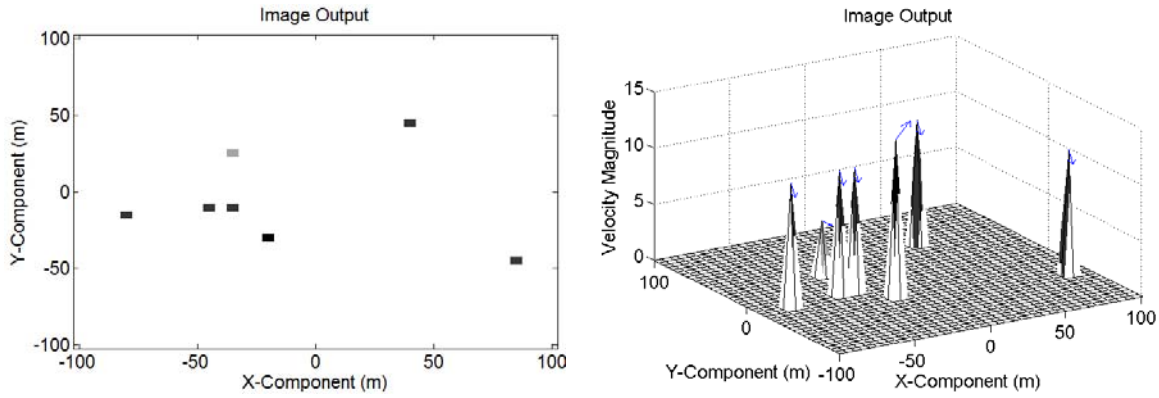

Figure 26. Image output of all expected velocity space

The three targets are accurately localized in both position and velocity. However, due to the image artifacts as shown in Figures 23, 24, and 25, the -3 dB threshold level is not sufficient to reject all image artifacts

E CONCLUSIONS AND RECOMMENDATIONS

This thesis analyzes the new imaging approach developed by *Cheney* and *Borden* [1] that can accommodate target motion during the imaging process. The simulation results, obtained by using MATLAB, showed that the new imaging scheme is well behaved. It is able to localize the target in position and velocity. In addition, the geometry of the transmitters, receivers, and waveforms utilized affect the behavior of the imaging system.

This thesis used single pulse radar waveforms, but in reality, fielded radar systems typically utilize long coded pulse trains. In addition, multistatic radar systems may not be restricted to one transmitter. In this case, the imaging scheme has to be adjusted to incorporate more realistic radar waveforms and optimized for the transmitter/receiver geometries for implementation of the imaging algorithm. These will be used to support the development of the eventual imaging algorithm. Finally, real world target data can then be applied to the developed imaging algorithm to assess its performance.

APPENDIX: MATLAB CODES

Scattering Data of Linear Array Configuration

```
close all
clear all
clc

%Origin of the image scene is set at (0,0)
%Target is set at (1km,1km) away from the origin with Velocity of (1,0)
%Transmitted is set at (-10km,0) away from the origin

%Target Information
tt=[-1000 0;-200 0;400 0]; %;0 840;50 50];            %Target X position, Y position
tt_vel=[0 0;0 0;0 0]; %;0 170;800 -850];      %Target velocity in X direction, Y direction
N_tt=length(tt(:,1));                %No of Targets

%Transmitter Information
Tx =[-10e3 0];          %Transmitter X position, Y position
N_Tx=length(Tx(:,1));                %No of Transmitter
T_tx=0;                 %Start time of transmitted pulse = always zero for the case of single
transmitter
Tx_mag=sqrt(Tx(1,1)^2+Tx(1,2)^2);
Tx_hat=Tx/sqrt(Tx(1,1)^2+Tx(1,2)^2);

%Receiver Information

%single line of 51 receivers at X=10e3 away from the origin.
Rx_x(1:51,1)=-10e3;
Rx_y=fliplr(-25000:1000:25000)';
Rx=[Rx_x Rx_y]; %Receiver position in X,Y co-ordinates
N_Rx=length(Rx(:,1));

Rx_mag= sqrt(Rx(:,1).*Rx(:,1)+Rx(:,2).*Rx(:,2));
Rx_hat(:,1)=Rx(:,1)./sqrt(Rx(:,1).*Rx(:,1)+Rx(:,2).*Rx(:,2));
Rx_hat(:,2)= Rx(:,2)./sqrt(Rx(:,1).*Rx(:,1)+Rx(:,2).*Rx(:,2));

%Signal information
c=3e8;
W_tx=2*pi*(10e9);      %Carrier Freq is 10GHz
K_tx=W_tx/c;          %Ky=Wy/c

%Waveform information
```

```
%pulse width of 0.2 us (30m of resolution and listening time of 100us (15km of Runamb)
% total period 100us

fs = 20e6;                                  % Using baseband signal of 1kHz. Therefore 20MHz
sampling. Nyquisting sampling rate
ts = 1/fs;
t1 = 0:1:20; %0:ts:1e-6; %0:1:20;               %pulse transmit time
t2 = 0:1:1979; %1e-6+ts:ts:100e-6; %0:1:1979;    %listening time
period = 100e-6;
T_period=0:ts:100e-6;
T=[t1 t2];                                  %period of 100us
s = [rectpuls(0,t1) zeros(1,length(t2))];       % 0.2 us Rect. pulse
S=fft(s);
w=(2*pi/period)*T;

TT_Data=zeros(1,2001);

%Generating Target Signal
for l=1:N_Tx              %For all Transmitter
   for m=1:N_Rx           %For all Receiver
      for n=1:N_tt        %For all targets
         tau=                        T_tx+(((Tx_mag(l,:)-(Tx_hat(l,:)*tt(n,:)'))+(Rx_mag(m,:)-
(Rx_hat(m,:)*tt(n,:)')))/c);%time delay
         phi=K_tx*Rx_mag(m,:)-
K_tx*(Tx_hat(l,:)+Rx_hat(m,:))*(tt(n,:)+((Rx_hat(m,:)*(Rx(m,:)-tt(n,:))')*tt_vel(n,:)/c))';
         alpha=1-(Tx_hat(l,:)+Rx_hat(m,:))*(tt_vel(n,:)/c)';
         TT_Data = TT_Data + exp(i*phi)*exp(i*W_tx*alpha*T).*ifft(S.*exp(-i*w*tau));
      end
   end
end

figure
plot(T_period,abs(TT_Data));
```

Scattering Data of Circular Array Configuration

```
close all
clear all
clc

%Origin of the image scene is set at (0,0)
%Target is set at (1km,1km) away from the origin with Velocity of (1,0)
%Transmitted is set at (-10km,0) away from the origin
```

```
%Target Information
tt=[-1000 0;-200 0;400 0]; %;0 840;50 50];            %Target X position, Y position
tt_vel=[0 0;0 0;0 0]; %;0 170;800 -850];      %Target velocity in X direction, Y direction
N_tt=length(tt(:,1));                %No of Targets

%Transmitter Information
Tx =[-10e3 0];          %Transmitter X position, Y position
N_Tx=length(Tx(:,1));                %No of Transmitter
T_tx=0;                 %Start time of transmitted pulse = always zero for the case of single
transmitter
Tx_mag=sqrt(Tx(1,1)^2+Tx(1,2)^2);
Tx_hat=Tx/sqrt(Tx(1,1)^2+Tx(1,2)^2);

%Receiver Information
%Receiver in Circular Configuration at 10km away from the origin.
theta=0:.125:2*pi;
[Rx_x Rx_y]=pol2cart(theta,10e3); %R is 10km away from origin
Rx=[Rx_x' Rx_y']; %Receiver position in X,Y co-ordinates
N_Rx=length(Rx(:,1));

Rx_mag= sqrt(Rx(:,1).*Rx(:,1)+Rx(:,2).*Rx(:,2));
Rx_hat(:,1)=Rx(:,1)./sqrt(Rx(:,1).*Rx(:,1)+Rx(:,2).*Rx(:,2));
Rx_hat(:,2)= Rx(:,2)./sqrt(Rx(:,1).*Rx(:,1)+Rx(:,2).*Rx(:,2));

%Signal information
c=3e8;
W_tx=2*pi*(10e9);      %Carrier Freq is 10GHz
K_tx=W_tx/c;          %Ky=Wy/c

%Waveform information
%pulse width of 0.2 us (30m of resolution and listening time of 100us (15km of Runamb)
% total period 100us

fs = 20e6;                                % Using baseband signal of 1kHz. Therefore 20MHz
sampling. Nyquisting sampling rate
ts = 1/fs;
t1 = 0:1:20; %0:ts:1e-6; %0:1:20;              %pulse transmit time
t2 = 0:1:1979; %1e-6+ts:ts:100e-6; %0:1:1979;    %listening time
period = 100e-6;
T_period=0:ts:100e-6;
T=[t1 t2];                                %period of 100us
s = [rectpuls(0,t1) zeros(1,length(t2))];        % 0.2 us Rect. pulse
S=fft(s);
w=(2*pi/period)*T;
```

```
TT_Data=zeros(1,2001);

%Generating Target Signal
for l=1:N_Tx              %For all Transmitter
   for m=1:N_Rx           %For all Receiver
      for n=1:N_tt        %For all targets
         tau=                    T_tx+(((Tx_mag(l,:)-(Tx_hat(l,:)*tt(n,:)'))+(Rx_mag(m,:)-
(Rx_hat(m,:)*tt(n,:)')))/c);%time delay
         phi=K_tx*Rx_mag(m,:)-
K_tx*(Tx_hat(l,:)+Rx_hat(m,:))*(tt(n,:)+((Rx_hat(m,:)*(Rx(m,:)-tt(n,:))')*tt_vel(n,:)/c))';
         alpha=1-(Tx_hat(l,:)+Rx_hat(m,:))*(tt_vel(n,:)/c)';
         TT_Data = TT_Data + exp(i*phi)*exp(i*W_tx*alpha*T).*ifft(S.*exp(-i*w*tau));
      end
   end
end

plot(T_period,abs(TT_Data));
```

Position PSF of Linear Array Configuration Using Rectangular Pulse

```
clear all
close all
clc

%%  Variables to be specified
tt=[0 0];              % actual target - tt
tt_vel=[0 0];              % actual target velocity - tt_vel

%Transmitter
Tx=[-10e3 0];
N_Tx=length(Tx(:,1));
Tx_mag=sqrt(Tx(1,1)^2+Tx(1,2)^2);
Tx_hat=Tx/sqrt(Tx(1,1)^2+Tx(1,2)^2);

%Receiver
Rx_x(1:51,1)=-10e3;
Rx_y=fliplr(-25000:1000:25000)';
Rx=[Rx_x Rx_y]; %Receiver position in X,Y co-ordinates
N_Rx=length(Rx(:,1));
Rx_mag= sqrt(Rx(:,1).*Rx(:,1)+Rx(:,2).*Rx(:,2));
Rx_hat(:,1)=Rx(:,1)./sqrt(Rx(:,1).*Rx(:,1)+Rx(:,2).*Rx(:,2));
Rx_hat(:,2)= Rx(:,2)./sqrt(Rx(:,1).*Rx(:,1)+Rx(:,2).*Rx(:,2));
```

```
E_tt_vel=[0 0];

%%  Parameters Defined
P_Width= 1e-6;

J=1;                    % Jacobian
c=3*10^8;
k_y=2*pi*(10e9)/c;        % wave vector @f=10 GHz

%Expected Target Position
res=1;
E_tt_x=-50:res:50;     %Sampled by Range Resolution
E_tt_y=-100:res:100;     %Sampled by Range Resolution
E_tt_y=fliplr(E_tt_y);

value=0;
for g=1:length(E_tt_y)
   for h=1:length(E_tt_x)
   E_tt=[E_tt_x(1,h) E_tt_y(1,g)];
      for l=1:N_Tx        %For all Transmitter
         for m=1:N_Rx    %For all Receiver
            arg1=(Tx_hat(l,:)+Rx_hat(m,:))*((E_tt_vel*(Rx_hat(m,:)*E_tt'))-
(tt_vel*(Rx_hat(m,:)*tt')))';
            phase1=exp(-i*k_y*arg1/c);
            arg2=(Tx_hat(l,:)+Rx_hat(m,:))*((E_tt-tt)+(0.5*(E_tt_vel-
tt_vel)*((Tx_hat(l,:)+Rx_hat(m,:))*(E_tt+tt)')))';
            phase2=exp(i*k_y*arg2/c);
            tau=((Tx_hat(l,:)+Rx_hat(m,:))*(E_tt-tt)')/c;
            if abs(tau)<P_Width
               neu= k_y*((Tx_hat(l,:)+Rx_hat(m,:))*(E_tt_vel-tt_vel)');
               amb=pi*(P_Width-abs(tau))*exp(-i*0.5*neu*P_Width)*sinc((0.5/pi)*(-
neu)*(P_Width-abs(tau)));
            else
               amb=0;
            end
            value= value + phase1*phase2*amb*J;
         end
      end
      k(g,h)=value.^2;
      value=0;
   end
end

K=abs(k)/max(max(abs(k)));
```

```
KT=K-0.707;
K_3db=(KT>0).*K;

figure
imagesc(E_tt_x,E_tt_y,abs(k))
title('Position PSF of Linear Array of Receivers');

figure
imagesc(E_tt_x,E_tt_y,K)
colormap(gray);
title('Position PSF of Linear Array of Receivers - Normalised');

figure
imagesc(E_tt_x,E_tt_y,K_3db)
colormap(gray);
title('Position PSF of Linear Array of Receivers - Normalised @ 3dB Threshold');
```

Velocity PSF of Linear Array Configuration Using Rectangular Pulse

```
close all
clear all
clc

%%  Variables to be specified

% Actual Target Position and Velocity
tt=[0 0];               % actual target - tt
tt_vel=[0 0];               % actual target velocity - tt_vel

% Transmitter location
Tx=[-10e3 0];
N_Tx=length(Tx(:,1));
Tx_mag=sqrt(Tx(1,1)^2+Tx(1,2)^2);
Tx_hat=Tx/sqrt(Tx(1,1)^2+Tx(1,2)^2);

%Receiver Location
Rx_x(1:51,1)=-10e3;
Rx_y=fliplr(-25000:1000:25000)';
Rx=[Rx_x Rx_y]; %Receiver position in X,Y co-ordinates
N_Rx=length(Rx(:,1));
Rx_mag= sqrt(Rx(:,1).*Rx(:,1)+Rx(:,2).*Rx(:,2));
Rx_hat(:,1)=Rx(:,1)./sqrt(Rx(:,1).*Rx(:,1)+Rx(:,2).*Rx(:,2));
Rx_hat(:,2)= Rx(:,2)./sqrt(Rx(:,1).*Rx(:,1)+Rx(:,2).*Rx(:,2));
```

```
E_tt=[0 0];
P_Width=1e-6;

%%  Parameters Defined
J=1;                    % Jacobian
c=3*10^8;
k_y=2*pi*(10e9)/c;        % wave vector @f=10 GHz

%%  PSF Velocity Defined
res=1;
E_tt_vel_x=-150:res:150;    %Sampled by Range Resolution
E_tt_vel_y=-150:res:150;    %Sampled by Range Resolution
E_tt_vel_y=fliplr(E_tt_vel_y);

value=0;
for g=1:length(E_tt_vel_y)
   for h=1:length(E_tt_vel_x)
   E_tt_vel=[E_tt_vel_x(1,h) E_tt_vel_y(1,g)];
      for l=1:N_Tx       %For all Transmitter
         for m=1:N_Rx    %For all Receiver
            arg1=(Tx_hat(l,:)+Rx_hat(m,:))*((E_tt_vel*(Rx_hat(m,:)*E_tt'))-
(tt_vel*(Rx_hat(m,:)*tt')))';
            phase1=exp(-i*k_y*arg1/c);
            arg2=(Tx_hat(l,:)+Rx_hat(m,:))*((E_tt-tt)+(0.5*(E_tt_vel-
tt_vel)*((Tx_hat(l,:)+Rx_hat(m,:))*(E_tt+tt)')))';
            phase2=exp(i*k_y*arg2/c);
            tau=((Tx_hat(l,:)+Rx_hat(m,:))*(E_tt-tt)')/c;
            if abs(tau)<P_Width
               neu= k_y*((Tx_hat(l,:)+Rx_hat(m,:))*(E_tt_vel-tt_vel)');
               amb=pi*(P_Width-abs(tau))*exp(-i*0.5*neu*P_Width)*sinc((0.5/pi)*(-
neu)*(P_Width-abs(tau)));
            else
               amb=0;
            end
            value= value + phase1*phase2*amb*J;
         end
      end
      k(g,h)=value.^2;
      value=0;
   end
end

K=abs(k)/max(max(abs(k)));
```

```
KT=K-0.99995;
K_3db=(KT>0).*K;

figure
imagesc(E_tt_vel_x,E_tt_vel_y,abs(k))
title('Velocity PSF of Linear Array of Receivers');

figure
imagesc(E_tt_vel_x,E_tt_vel_y,K)
title('Velocity PSF of Linear Array of Receivers - Normalised');

figure
imagesc(E_tt_vel_x,E_tt_vel_y,K_3db)
colormap(gray);
title('Velocity PSF of Linear Array of Receivers - Normalised @ 3dB Threshold');
```

Position PSF of Circular Array Configuration Using Rectangular Pulse

```
close all
clear all
clc

%%  Variables to be specified
tt=[0 0];               % actual target
tt_vel=[0 0];               % actual target velocity

%Transmitter
Tx=[-10e3 0];
N_Tx=length(Tx(:,1));
Tx_mag=sqrt(Tx(1,1)^2+Tx(1,2)^2);
Tx_hat=Tx/sqrt(Tx(1,1)^2+Tx(1,2)^2);

%Receiver in Circular Configuration at 10km away from the origin.
theta=0:.125:2*pi;
[Rx_x Rx_y]=pol2cart(theta,10e3); %R is 10km away from origin
Rx=[Rx_x' Rx_y']; %Receiver position in X,Y co-ordinates
N_Rx=length(Rx(:,1));

Rx_mag= sqrt(Rx(:,1).*Rx(:,1)+Rx(:,2).*Rx(:,2));
Rx_hat(:,1)=Rx(:,1)./sqrt(Rx(:,1).*Rx(:,1)+Rx(:,2).*Rx(:,2));
Rx_hat(:,2)= Rx(:,2)./sqrt(Rx(:,1).*Rx(:,1)+Rx(:,2).*Rx(:,2));

E_tt_vel=[0 0];
```

```
%%  Parameters Defined
P_Width=1e-6;

J=1;                    % Jacobian
c=3*10^8;
k_y=2*pi*(10e9)/c;        % wave vector @f=10 GHz

%Expected Target Position
res=1;
E_tt_x=-200:res:200;    %Sampled by Range Resolution
E_tt_y=-200:res:200;    %Sampled by Range Resolution
E_tt_y=fliplr(E_tt_y);

value=0;
for g=1:length(E_tt_y)
   for h=1:length(E_tt_x)
   E_tt=[E_tt_x(1,h) E_tt_y(1,g)];
      for l=1:N_Tx       %For all Transmitter
         for m=1:N_Rx    %For all Receiver
            arg1=(Tx_hat(l,:)+Rx_hat(m,:))*((E_tt_vel*(Rx_hat(m,:)*E_tt'))-
(tt_vel*(Rx_hat(m,:)*tt')))';
            phase1=exp(-i*k_y*arg1/c);
            arg2=(Tx_hat(l,:)+Rx_hat(m,:))*((E_tt-tt)+(0.5*(E_tt_vel-
tt_vel)*((Tx_hat(l,:)+Rx_hat(m,:))*(E_tt+tt)')))';
            phase2=exp(i*k_y*arg2/c);
            tau=((Tx_hat(l,:)+Rx_hat(m,:))*(E_tt-tt)')/c;
             if abs(tau)<P_Width
               neu= k_y*((Tx_hat(l,:)+Rx_hat(m,:))*(E_tt_vel-tt_vel)');
               amb=(P_Width-abs(tau))*exp(i*0.5*neu*(P_Width-
abs(tau)))*sinc(0.5*neu*(P_Width-abs(tau)));
            else
               amb=0;
            end
            value= value + phase1*phase2*amb*J;
         end
      end
      k(g,h)=value.^2;
      value=0;
   end
end

K=abs(k)/max(max(abs(k)));
KT=K-0.707;
K_3db=(KT>0).*K;
```

```
figure
imagesc(E_tt_x,E_tt_y,abs(k))
title('Position PSF of Circular Array of Receivers');

figure
imagesc(E_tt_x,E_tt_y,K)
title('Position PSF of Circular Array of Receivers - Normalised');

figure
imagesc(E_tt_x,E_tt_y,K_3db)
colormap(gray);
title('Position PSF of Circular Array of Receivers - Normalised @ 3dB Threshold');

filename=['Position PSF of Circular Array of Receivers - Normalised @ 3dB Threshold
Pulse Width ' num2str(P_Width)];
saveas(gcf,filename,'fig')
close
```

Velocity PSF of Circular Array Configuration Using Rectangular Pulse

```
% Actual Target Position and Velocity
tt=[0 0];               % actual target - tt
tt_vel=[0 0];               % actual target velocity - tt_vel

% Transmitter location
Tx=[-10e3 0];
N_Tx=length(Tx(:,1));
Tx_mag=sqrt(Tx(1,1)^2+Tx(1,2)^2);
Tx_hat=Tx/sqrt(Tx(1,1)^2+Tx(1,2)^2);

%Receiver in Circular Configuration at 10km away from the origin.
theta=0:.125:2*pi;
[Rx_x Rx_y]=pol2cart(theta,10e3); %R is 10km away from origin
Rx=[Rx_x' Rx_y']; %Receiver position in X,Y co-ordinates
N_Rx=length(Rx(:,1));

Rx_mag= sqrt(Rx(:,1).*Rx(:,1)+Rx(:,2).*Rx(:,2));
Rx_hat(:,1)=Rx(:,1)./sqrt(Rx(:,1).*Rx(:,1)+Rx(:,2).*Rx(:,2));
Rx_hat(:,2)= Rx(:,2)./sqrt(Rx(:,1).*Rx(:,1)+Rx(:,2).*Rx(:,2));

E_tt=[0 0];
% P_Width=1e-6;
% gamma=0.5e12;
```

```
%%  Parameters Defined
J=1;                    % Jacobian
c=3*10^8;
k_y=2*pi*(10e9)/c;        % wave vector @f=10 GHz

%%  PSF Velocity Defined
res=1;
E_tt_vel_x=-200:res:200;     %Sampled by Range Resolution
E_tt_vel_y=-200:res:200;     %Sampled by Range Resolution
E_tt_vel_y=fliplr(E_tt_vel_y);

value=0;
for g=1:length(E_tt_vel_y)
   for h=1:length(E_tt_vel_x)
   E_tt_vel=[E_tt_vel_x(1,h) E_tt_vel_y(1,g)];
      for l=1:N_Tx        %For all Transmitter
         for m=1:N_Rx    %For all Receiver
            arg1=(Tx_hat(l,:)+Rx_hat(m,:))*((E_tt_vel*(Rx_hat(m,:)*E_tt'))-
(tt_vel*(Rx_hat(m,:)*tt')))';
            phase1=exp(-i*k_y*arg1/c);
            arg2=(Tx_hat(l,:)+Rx_hat(m,:))*((E_tt-tt)+(0.5*(E_tt_vel-
tt_vel)*((Tx_hat(l,:)+Rx_hat(m,:))*(E_tt+tt')))';
            phase2=exp(i*k_y*arg2/c);
            tau=((Tx_hat(l,:)+Rx_hat(m,:))*(E_tt-tt)')/c;
            if abs(tau)<P_Width
               neu= k_y*((Tx_hat(l,:)+Rx_hat(m,:))*(E_tt_vel-tt_vel)');
               amb=(P_Width-abs(tau))*exp(i*0.5*(neu+gamma*tau)*(P_Width-
abs(tau)))*sinc(0.5*(neu+gamma*tau)*(P_Width-abs(tau)));
            else
               amb=0;
            end
            value= value + phase1*phase2*amb*J;
         end
      end
      k(g,h)=value.^2;
      value=0;
   end
end

K=abs(k)/max(max(abs(k)));
KT=K-0.707;
K_3db=(KT>0).*K;
```

```
figure
imagesc(E_tt_vel_x,E_tt_vel_y,abs(k))
title('Position PSF of Linear Array of Receivers');

figure
imagesc(E_tt_vel_x,E_tt_vel_y,K)
title('Position PSF of Linear Array of Receivers - Normalised');

figure
imagesc(E_tt_vel_x,E_tt_vel_y,K_3db)
colormap(gray);
title('Velocity PSF of Circular Array of Receivers - Normalised @ 3dB Threshold');

filename=['Velocity PSF of Circular Array of Receivers Pulse Width' num2str(P_Width)
'- Normalised @ 3dB Threshold Chirp Rate' num2str(gamma)];
saveas(gcf,filename,'fig')
close
```

Position PSF of Linear Array Configuration Using Chirp Pulse

```
%%  Variables to be specified
tt=[0 0];                % actual target - tt
tt_vel=[0 0];              % actual target velocity - tt_vel

%Transmitter
Tx=[-10e3 0];
N_Tx=length(Tx(:,1));
Tx_mag=sqrt(Tx(1,1)^2+Tx(1,2)^2);
Tx_hat=Tx/sqrt(Tx(1,1)^2+Tx(1,2)^2);

%Receiver
Rx_x(1:51,1)=-10e3;
Rx_y=fliplr(-25000:1000:25000)';
Rx=[Rx_x Rx_y]; %Receiver position in X,Y co-ordinates
N_Rx=length(Rx(:,1));
Rx_mag= sqrt(Rx(:,1).*Rx(:,1)+Rx(:,2).*Rx(:,2));
Rx_hat(:,1)=Rx(:,1)./sqrt(Rx(:,1).*Rx(:,1)+Rx(:,2).*Rx(:,2));
Rx_hat(:,2)= Rx(:,2)./sqrt(Rx(:,1).*Rx(:,1)+Rx(:,2).*Rx(:,2));

%%  Parameters Defined
E_tt_vel=[0 0];
% P_Width= 1e-6; %Pulse Width
% gamma = 0.5e12; %Chirp Rate
```

```
J=1;                    % Jacobian
c=3*10^8;
k_y=2*pi*(10e9)/c;        % wave vector @f=10 GHz

%Expected Target Position
res=1;
E_tt_x=-200:res:200;    %Sampled by Range Resolution
E_tt_y=-200:res:200;    %Sampled by Range Resolution
E_tt_y=fliplr(E_tt_y);

value=0;
for g=1:length(E_tt_y)
   for h=1:length(E_tt_x)
   E_tt=[E_tt_x(1,h) E_tt_y(1,g)];
      for l=1:N_Tx       %For all Transmitter
         for m=1:N_Rx    %For all Receiver
            arg1=(Tx_hat(l,:)+Rx_hat(m,:))*((E_tt_vel*(Rx_hat(m,:)*E_tt'))-
(tt_vel*(Rx_hat(m,:)*tt')))';
            phase1=exp(-i*k_y*arg1/c);
            arg2=(Tx_hat(l,:)+Rx_hat(m,:))*((E_tt-tt)+(0.5*(E_tt_vel-
tt_vel)*((Tx_hat(l,:)+Rx_hat(m,:))*(E_tt+tt)')))';
            phase2=exp(i*k_y*arg2/c);
            tau=((Tx_hat(l,:)+Rx_hat(m,:))*(E_tt-tt)')/c;
            if abs(tau)<P_Width
               neu= k_y*((Tx_hat(l,:)+Rx_hat(m,:))*(E_tt_vel-tt_vel)');
               amb=(P_Width-abs(tau))*exp(i*0.5*(neu+gamma*tau)*(P_Width-
abs(tau)))*sinc(0.5*(neu+gamma*tau)*(P_Width-abs(tau)));
            else
               amb=0;
            end
            value= value + phase1*phase2*amb*J;
         end
      end
      k(g,h)=value.^2;
      value=0;
   end
end

K=abs(k)/max(max(abs(k)));

KT=K-0.707;
K_3db=(KT>0).*K;

figure
```

```
imagesc(E_tt_x,E_tt_y,abs(k))
title('Position PSF of Linear Array of Receivers');

figure
imagesc(E_tt_x,E_tt_y,K)
colormap(gray);
title('Position PSF of Linear Array of Receivers - Normalised');

figure
imagesc(E_tt_x,E_tt_y,K_3db)
colormap(gray);
title('Position PSF of Linear Array of Receivers - Normalised @ 3dB Threshold');

filename=['Position PSF of Linear Array of Receivers Pulse Width' num2str(P_Width) '-
Normalised @ 3dB Threshold Chirp Rate' num2str(gamma)];
saveas(gcf,filename,'fig')
close
```

Velocity PSF of Linear Array Configuration Using Chirp Pulse

```
% Actual Target Position and Velocity
tt=[0 0];               % actual target - tt
tt_vel=[0 0];               % actual target velocity - tt_vel

% Transmitter location
Tx=[-10e3 0];
N_Tx=length(Tx(:,1));
Tx_mag=sqrt(Tx(1,1)^2+Tx(1,2)^2);
Tx_hat=Tx/sqrt(Tx(1,1)^2+Tx(1,2)^2);

%Receiver Location
Rx_x(1:51,1)=-10e3;
Rx_y=fliplr(-25000:1000:25000)';
Rx=[Rx_x Rx_y]; %Receiver position in X,Y co-ordinates
N_Rx=length(Rx(:,1));
Rx_mag= sqrt(Rx(:,1).*Rx(:,1)+Rx(:,2).*Rx(:,2));
Rx_hat(:,1)=Rx(:,1)./sqrt(Rx(:,1).*Rx(:,1)+Rx(:,2).*Rx(:,2));
Rx_hat(:,2)= Rx(:,2)./sqrt(Rx(:,1).*Rx(:,1)+Rx(:,2).*Rx(:,2));

%%  Parameters Defined
E_tt=[0 0];
% P_Width=50e-6;
% gamma=10e12;
```

```
J=1;                    % Jacobian
c=3*10^8;
k_y=2*pi*(10e9)/c;        % wave vector @f=10 GHz

%%  PSF Velocity Defined
res=1;
E_tt_vel_x=-200:res:200;     %Sampled by Velocity Resolution
E_tt_vel_y=-200:res:200;     %Sampled by Velocity Resolution
E_tt_vel_y=fliplr(E_tt_vel_y);

value=0;
for g=1:length(E_tt_vel_y)
   for h=1:length(E_tt_vel_x)
   E_tt_vel=[E_tt_vel_x(1,h) E_tt_vel_y(1,g)];
      for l=1:N_Tx        %For all Transmitter
         for m=1:N_Rx    %For all Receiver
            arg1=(Tx_hat(l,:)+Rx_hat(m,:))*((E_tt_vel*(Rx_hat(m,:)*E_tt'))-
(tt_vel*(Rx_hat(m,:)*tt')))';
            phase1=exp(-i*k_y*arg1/c);
            arg2=(Tx_hat(l,:)+Rx_hat(m,:))*((E_tt-tt)+(0.5*(E_tt_vel-
tt_vel)*((Tx_hat(l,:)+Rx_hat(m,:))*(E_tt+tt)')))';
            phase2=exp(i*k_y*arg2/c);
            tau=((Tx_hat(l,:)+Rx_hat(m,:))*(E_tt-tt)')/c;
            if abs(tau)<P_Width
               neu= k_y*((Tx_hat(l,:)+Rx_hat(m,:))*(E_tt_vel-tt_vel)');
               amb=(P_Width-abs(tau))*exp(i*0.5*(neu+gamma*tau)*(P_Width-
abs(tau)))*sinc(0.5*(neu+gamma*tau)*(P_Width-abs(tau)));
            else
               amb=0;
            end
            value= value + phase1*phase2*amb*J;
         end
      end
      k(g,h)=value.^2;
      value=0;
   end
end

K=abs(k)/max(max(abs(k)));
KT=K-0.707;
K_3db=(KT>0).*K;

figure
imagesc(E_tt_vel_x,E_tt_vel_y,abs(k))
```

```
title('Velocity PSF of Linear Array of Receivers');

figure
imagesc(E_tt_vel_x,E_tt_vel_y,K)
title('Velocity PSF of Linear Array of Receivers - Normalised');

figure
imagesc(E_tt_vel_x,E_tt_vel_y,K_3db)
colormap(gray);
title('Velocity PSF of Linear Array of Receivers - Normalised @ 3dB Threshold');

filename=['Velocity PSF of Linear Array of Receivers Pulse Width' num2str(P_Width) '-
Normalised @ 3dB Threshold Chirp Rate' num2str(gamma)];
saveas(gcf,filename,'fig')
close
```

Position PSF of Circular Array Configuration Using Chirp Pulse

```
%%  Variables to be specified
tt=[0 0];               % actual target
tt_vel=[0 0];               % actual target velocity

%Transmitter
Tx=[-10e3 0];
N_Tx=length(Tx(:,1));
Tx_mag=sqrt(Tx(1,1)^2+Tx(1,2)^2);
Tx_hat=Tx/sqrt(Tx(1,1)^2+Tx(1,2)^2);

%Receiver in Circular Configuration at 10km away from the origin.
theta=0:.125:2*pi;
[Rx_x Rx_y]=pol2cart(theta,10e3); %R is 10km away from origin
Rx=[Rx_x' Rx_y']; %Receiver position in X,Y co-ordinates
N_Rx=length(Rx(:,1));

Rx_mag= sqrt(Rx(:,1).*Rx(:,1)+Rx(:,2).*Rx(:,2));
Rx_hat(:,1)=Rx(:,1)./sqrt(Rx(:,1).*Rx(:,1)+Rx(:,2).*Rx(:,2));
Rx_hat(:,2)= Rx(:,2)./sqrt(Rx(:,1).*Rx(:,1)+Rx(:,2).*Rx(:,2));

E_tt_vel=[0 0];

%%  Parameters Defined
% P_Width=1e-6;
% gamma=0.5e12;
```

```
J=1;                    % Jacobian
c=3*10^8;
k_y=2*pi*(10e9)/c;        % wave vector @f=10 GHz

%Expected Target Position
res=1;
E_tt_x=-200:res:200;    %Sampled by Range Resolution
E_tt_y=-200:res:200;    %Sampled by Range Resolution
E_tt_y=fliplr(E_tt_y);

value=0;
for g=1:length(E_tt_y)
   for h=1:length(E_tt_x)
   E_tt=[E_tt_x(1,h) E_tt_y(1,g)];
      for l=1:N_Tx       %For all Transmitter
         for m=1:N_Rx    %For all Receiver
            arg1=(Tx_hat(l,:)+Rx_hat(m,:))*((E_tt_vel*(Rx_hat(m,:)*E_tt'))-
(tt_vel*(Rx_hat(m,:)*tt')))';
            phase1=exp(-i*k_y*arg1/c);
            arg2=(Tx_hat(l,:)+Rx_hat(m,:))*((E_tt-tt)+(0.5*(E_tt_vel-
tt_vel)*((Tx_hat(l,:)+Rx_hat(m,:))*(E_tt+tt)')))';
            phase2=exp(i*k_y*arg2/c);
            tau=((Tx_hat(l,:)+Rx_hat(m,:))*(E_tt-tt)')/c;
             if abs(tau)<P_Width
               neu= k_y*((Tx_hat(l,:)+Rx_hat(m,:))*(E_tt_vel-tt_vel)');
               amb=(P_Width-abs(tau))*exp(i*0.5*(neu+gamma*tau)*(P_Width-
abs(tau)))*sinc(0.5*(neu+gamma*tau)*(P_Width-abs(tau)));
            else
               amb=0;
            end
            value= value + phase1*phase2*amb*J;
         end
      end
      k(g,h)=value.^2;
      value=0;
   end
end

K=abs(k)/max(max(abs(k)));
KT=K-0.707;
K_3db=(KT>0).*K;

figure
imagesc(E_tt_x,E_tt_y,abs(k))
```

```
title('Position PSF of Circular Array of Receivers');

figure
imagesc(E_tt_x,E_tt_y,K)
title('Position PSF of Circular Array of Receivers - Normalised');

figure
imagesc(E_tt_x,E_tt_y,K_3db)
colormap(gray);
title('Position PSF of Circular Array of Receivers - Normalised @ 3dB Threshold');

filename=['Position PSF of Circular Array of Receivers Pulse Width' num2str(P_Width)
'- Normalised @ 3dB Threshold Chirp Rate' num2str(gamma)];
saveas(gcf,filename,'fig')
close
```

Velocity PSF of Circular Array Configuration Using Chirp Pulse

```
%%  Variables to be specified

% Actual Target Position and Velocity
tt=[0 0];               % actual target - tt
tt_vel=[0 0];               % actual target velocity - tt_vel

% Transmitter location
Tx=[-10e3 0];
N_Tx=length(Tx(:,1));
Tx_mag=sqrt(Tx(1,1)^2+Tx(1,2)^2);
Tx_hat=Tx/sqrt(Tx(1,1)^2+Tx(1,2)^2);

%Receiver in Circular Configuration at 10km away from the origin.
theta=0:.125:2*pi;
[Rx_x Rx_y]=pol2cart(theta,10e3); %R is 10km away from origin
Rx=[Rx_x' Rx_y']; %Receiver position in X,Y co-ordinates
N_Rx=length(Rx(:,1));

Rx_mag= sqrt(Rx(:,1).*Rx(:,1)+Rx(:,2).*Rx(:,2));
Rx_hat(:,1)=Rx(:,1)./sqrt(Rx(:,1).*Rx(:,1)+Rx(:,2).*Rx(:,2));
Rx_hat(:,2)= Rx(:,2)./sqrt(Rx(:,1).*Rx(:,1)+Rx(:,2).*Rx(:,2));

E_tt=[0 0];
% P_Width=1e-6;
% gamma=0.5e12;
```

```
%%  Parameters Defined
J=1;                    % Jacobian
c=3*10^8;
k_y=2*pi*(10e9)/c;        % wave vector @f=10 GHz

%%  PSF Velocity Defined
res=1;
E_tt_vel_x=-200:res:200;     %Sampled by Range Resolution
E_tt_vel_y=-200:res:200;     %Sampled by Range Resolution
E_tt_vel_y=fliplr(E_tt_vel_y);

value=0;
for g=1:length(E_tt_vel_y)
   for h=1:length(E_tt_vel_x)
   E_tt_vel=[E_tt_vel_x(1,h) E_tt_vel_y(1,g)];
      for l=1:N_Tx        %For all Transmitter
         for m=1:N_Rx    %For all Receiver
            arg1=(Tx_hat(l,:)+Rx_hat(m,:))*((E_tt_vel*(Rx_hat(m,:)*E_tt'))-
(tt_vel*(Rx_hat(m,:)*tt')))';
            phase1=exp(-i*k_y*arg1/c);
            arg2=(Tx_hat(l,:)+Rx_hat(m,:))*((E_tt-tt)+(0.5*(E_tt_vel-
tt_vel)*((Tx_hat(l,:)+Rx_hat(m,:))*(E_tt+tt)')))';
            phase2=exp(i*k_y*arg2/c);
            tau=((Tx_hat(l,:)+Rx_hat(m,:))*(E_tt-tt)')/c;
            if abs(tau)<P_Width
               neu= k_y*((Tx_hat(l,:)+Rx_hat(m,:))*(E_tt_vel-tt_vel)');
               amb=(P_Width-abs(tau))*exp(i*0.5*(neu+gamma*tau)*(P_Width-
abs(tau)))*sinc(0.5*(neu+gamma*tau)*(P_Width-abs(tau)));
            else
               amb=0;
            end
            value= value + phase1*phase2*amb*J;
         end
      end
      k(g,h)=value.^2;
      value=0;
   end
end

K=abs(k)/max(max(abs(k)));
KT=K-0.707;
K_3db=(KT>0).*K;

figure
```

```
imagesc(E_tt_vel_x,E_tt_vel_y,abs(k))
title('Position PSF of Linear Array of Receivers');

figure
imagesc(E_tt_vel_x,E_tt_vel_y,K)
title('Position PSF of Linear Array of Receivers - Normalised');

figure
imagesc(E_tt_vel_x,E_tt_vel_y,K_3db)
colormap(gray);
title('Velocity PSF of Circular Array of Receivers - Normalised @ 3dB Threshold');

filename=['Velocity PSF of Circular Array of Receivers Pulse Width' num2str(P_Width)
'- Normalised @ 3dB Threshold Chirp Rate' num2str(gamma)];
saveas(gcf,filename,'fig')
close
```

Imaging: Linear Array Configurations.

```
close all
clear all
clc

%Origin of the image scene is set at (0,0)
%Target is set at (1km,1km) away from the origin with Velocity of (1,0)
%Transmitted is set at (-10km,0) away from the origin

%Target Information
tt=[-35 25;-20 -30;40 45]; %;0 840;50 50];          %Target X position, Y position
tt_vel=[0 -5;10 10;-5 -10]; %;0 170;800 -850];      %Target velocity in X direction, Y
direction
N_tt=length(tt(:,1));              %No of Targets

%Transmitter Information
Tx =[-10e3 0];         %Transmitter X position, Y position
N_Tx=length(Tx(:,1));              %No of Transmitter
T_tx=0;                %Start time of transmitted pulse = always zero for the case of single
transmitter
Tx_mag=sqrt(Tx(1,1)^2+Tx(1,2)^2);
Tx_hat=Tx/sqrt(Tx(1,1)^2+Tx(1,2)^2);

%Receiver Information
%single line of 51 receivers at X=10e3 away from the origin.
Rx_x(1:51,1)=-10e3;
```

```
Rx_y=fliplr(-25000:1000:25000)';
Rx=[Rx_x Rx_y]; %Receiver position in X,Y co-ordinates
N_Rx=length(Rx(:,1));

Rx_mag= sqrt(Rx(:,1).*Rx(:,1)+Rx(:,2).*Rx(:,2));
Rx_hat(:,1)=Rx(:,1)./sqrt(Rx(:,1).*Rx(:,1)+Rx(:,2).*Rx(:,2));
Rx_hat(:,2)= Rx(:,2)./sqrt(Rx(:,1).*Rx(:,1)+Rx(:,2).*Rx(:,2));

%Signal information
c=3e8;
W_tx=2*pi*(10e9);      %Carrier Freq is 10GHz
K_tx=W_tx/c;          %Ky=Wy/c

%Waveform information
%pulse width of 0.2 us (30m of resolution and listening time of 100us (15km of Runamb)
% total period 100us

fs = 20e6;                                % Using baseband signal of 1kHz. Therefore 20MHz
sampling. Nyquisting sampling rate
ts = 1/fs;
t1 = 0:1:20; %0:ts:1e-6; %0:1:20;              %pulse transmit time
t2 = 0:1:1979; %1e-6+ts:ts:100e-6; %0:1:1979;    %listening time
period = 100e-6;
T_period=0:ts:100e-6;
T=[t1 t2];                                %period of 100us
s = [rectpuls(0,t1) zeros(1,length(t2))];       % 0.2 us Rect. pulse
S=fft(s);
w=(2*pi/period)*T;

TT_Data=zeros(1,2001);

%Generating Target Signal
for l=1:N_Tx              %For all Transmitter
   for m=1:N_Rx           %For all Receiver
      for n=1:N_tt        %For all targets
         tau=                    T_tx+(((Tx_mag(l,:)-(Tx_hat(l,:)*tt(n,:)'))+(Rx_mag(m,:)-
(Rx_hat(m,:)*tt(n,:)')))/c);%time delay
         phi=K_tx*Rx_mag(m,:)-
K_tx*(Tx_hat(l,:)+Rx_hat(m,:))*(tt(n,:)+((Rx_hat(m,:)*(Rx(m,:)-tt(n,:))')*tt_vel(n,:)/c))';
         alpha=1-(Tx_hat(l,:)+Rx_hat(m,:))*(tt_vel(n,:)/c)';
         TT_Data = TT_Data + exp(i*phi)*exp(i*W_tx*alpha*T).*ifft(S.*exp(-i*w*tau));
      end
   end
end
```

```
% figure
% plot(T_period,abs(TT_Data));

%Expected Target Position
E_tt_x=-100:5:100;     %Sampled by Range Resolution
E_tt_y=-100:5:100;     %Sampled by Range Resolution
E_tt_y=fliplr(E_tt_y);

Expected Target Velocity
E_tt_vel_x=-50:1:50;
E_tt_vel_y=-50:1:50;
E_tt_vel_y=fliplr(E_tt_vel_y);
L=length(E_tt_y)*length(E_tt_x);

%Generating Information Database
[X,Y]=meshgrid(E_tt_x,E_tt_y);
Vel_U=zeros(length(E_tt_x),length(E_tt_y));
Vel_V=zeros(length(E_tt_x),length(E_tt_y));
Vel_W=zeros(length(E_tt_x),length(E_tt_y));

nn=1;
This for loop is for spanning across vested velocity space
for u=1:length(E_tt_vel_y)
   for v=1:length(E_tt_vel_x)
      E_tt_vel=[E_tt_vel_x(1,v) E_tt_vel_y(1,u)];
      E_tt_vel_mag=sqrt(E_tt_vel(1,1)^2+E_tt_vel(1,2)^2);
      %Generating Expected Target Database
      for g=1:length(E_tt_y)
         for h=1:length(E_tt_x)
            E_tt=[E_tt_x(1,h) E_tt_y(1,g)];
            E_TT_Data=zeros(1,length(T));
            for l=1:N_Tx       %For all Transmitter
               for m=1:N_Rx    %For all Receiver
                  tau=          T_tx+(((Tx_mag(l,:)-(Tx_hat(l,:)*E_tt(1,:)'))+(Rx_mag(m,:)-
(Rx_hat(m,:)*E_tt(1,:)')))/c); %time delay
                  phi=K_tx*Rx_mag(m,:)-
K_tx*(Tx_hat(l,:)+Rx_hat(m,:))*(E_tt(1,:)+((Rx_hat(m,:)*(Rx(m,:)-
E_tt(1,:))')*E_tt_vel/c))';
                  alpha=1-(Tx_hat(l,:)+Rx_hat(m,:))*(E_tt_vel/c)';
                  E_TT_Data                =                E_TT_Data                +
exp(i*phi)*exp(i*W_tx*alpha*T).*ifft(S.*exp(-i*w*tau));
               end
            end
```

```
            I(g,h)=E_TT_Data*TT_Data';
        end
    end

    I_abs=abs(I);
    I_norm=I_abs/max(max(I_abs));
    I_tt=(I_norm-0.707);
    I_tt=ceil(I_tt)*E_tt_vel_mag;
    [row,col]=find(I_tt);
    Vel_U(row,col)=E_tt_vel(1,1);
    Vel_V(row,col)=E_tt_vel(1,2);
    if nn==1
        I_tt_sum=I_tt;
    else
        I_tt_sum=I_tt_sum+I_tt;
    end
    nn=nn+1;
  end
end

figure
surf(E_tt_x,E_tt_y,I_tt_sum); %or I_norm*E_tt_vel_mag
%title(['velocity Vector [', num2str(E_tt_vel),']']);
colorbar;
hold on
quiver3(X,Y,I_tt_sum,Vel_U,Vel_V,Vel_W);
```

Imaging: Circular Array Configurations.

```
close all
clear all
clc

%Origin of the image scene is set at (0,0)
%Target is set at (1km,1km) away from the origin with Velocity of (1,0)
%Transmitted is set at (-10km,0) away from the origin

%Target Information
tt=[-35 25;-20 -30;40 45]; %;0 840;50 50];          %Target X position, Y position
tt_vel=[0 -5;10 10;-5 -10]; %;0 170;800 -850];      %Target velocity in X direction, Y
direction
N_tt=length(tt(:,1));              %No of Targets

%Transmitter Information
```

```
Tx =[-10e3 0];          %Transmitter X position, Y position
N_Tx=length(Tx(:,1));               %No of Transmitter
T_tx=0;                 %Start time of transmitted pulse = always zero for the case of single
transmitter
Tx_mag=sqrt(Tx(1,1)^2+Tx(1,2)^2);
Tx_hat=Tx/sqrt(Tx(1,1)^2+Tx(1,2)^2);

%Receiver Information
%Receiver in Circular Configuration at 10km away from the origin.
theta=0:.125:2*pi;
[Rx_x Rx_y]=pol2cart(theta,10e3); %R is 10km away from origin
Rx=[Rx_x' Rx_y']; %Receiver position in X,Y co-ordinates
N_Rx=length(Rx(:,1));

Rx_mag= sqrt(Rx(:,1).*Rx(:,1)+Rx(:,2).*Rx(:,2));
Rx_hat(:,1)=Rx(:,1)./sqrt(Rx(:,1).*Rx(:,1)+Rx(:,2).*Rx(:,2));
Rx_hat(:,2)= Rx(:,2)./sqrt(Rx(:,1).*Rx(:,1)+Rx(:,2).*Rx(:,2));

%Signal information
c=3e8;
W_tx=2*pi*(10e9);      %Carrier Freq is 10GHz
K_tx=W_tx/c;           %Ky=Wy/c

%Waveform information
%pulse width of 0.2 us (30m of resolution and listening time of 100us (15km of Runamb)
% total period 100us

fs = 20e6;                                  % Using baseband signal of 1kHz. Therefore 20MHz
sampling. Nyquisting sampling rate
ts = 1/fs;
t1 = 0:1:20; %0:ts:1e-6; %0:1:20;               %pulse transmit time
t2 = 0:1:1979; %1e-6+ts:ts:100e-6; %0:1:1979;    %listening time
period = 100e-6;
T_period=0:ts:100e-6;
T=[t1 t2];                                  %period of 100us
s = [rectpuls(0,t1) zeros(1,length(t2))];       % 0.2 us Rect. pulse
S=fft(s);
w=(2*pi/period)*T;

TT_Data=zeros(1,2001);

%Generating Target Signal
for l=1:N_Tx              %For all Transmitter
   for m=1:N_Rx           %For all Receiver
```

```
      for n=1:N_tt       %For all targets
         tau=                        T_tx+(((Tx_mag(l,:)-(Tx_hat(l,:)*tt(n,:)'))+(Rx_mag(m,:)-
(Rx_hat(m,:)*tt(n,:)')))/c);%time delay
         phi=K_tx*Rx_mag(m,:)-
K_tx*(Tx_hat(l,:)+Rx_hat(m,:))*(tt(n,:)+((Rx_hat(m,:)*(Rx(m,:)-tt(n,:))')*tt_vel(n,:)/c))';
         alpha=1-(Tx_hat(l,:)+Rx_hat(m,:))*(tt_vel(n,:)/c)';
         TT_Data = TT_Data + exp(i*phi)*exp(i*W_tx*alpha*T).*ifft(S.*exp(-i*w*tau));
      end
   end
end

% figure
% plot(T_period,abs(TT_Data));

%Expected Target Position
E_tt_x=-100:5:100;     %Sampled by Range Resolution
E_tt_y=-100:5:100;     %Sampled by Range Resolution
E_tt_y=fliplr(E_tt_y);

%Expected Target Velocity
E_tt_vel_x=-50:1:50;
E_tt_vel_y=-50:1:50;
E_tt_vel_y=fliplr(E_tt_vel_y);
L=length(E_tt_y)*length(E_tt_x);

%Generating Information Database
[X,Y]=meshgrid(E_tt_x,E_tt_y);
Vel_U=zeros(length(E_tt_x),length(E_tt_y));
Vel_V=zeros(length(E_tt_x),length(E_tt_y));
Vel_W=zeros(length(E_tt_x),length(E_tt_y));

nn=1;
This for loop is for spanning across vested velocity space
for u=1:length(E_tt_vel_y)
   for v=1:length(E_tt_vel_x)
      E_tt_vel=[E_tt_vel_x(1,v) E_tt_vel_y(1,u)];
      E_tt_vel_mag=sqrt(E_tt_vel(1,1)^2+E_tt_vel(1,2)^2);
      %Generating Expected Target Database
      for g=1:length(E_tt_y)
         for h=1:length(E_tt_x)
            E_tt=[E_tt_x(1,h) E_tt_y(1,g)];
            E_TT_Data=zeros(1,length(T));
            for l=1:N_Tx       %For all Transmitter
               for m=1:N_Rx    %For all Receiver
```

```
                tau=          T_tx+(((Tx_mag(l,:)-(Tx_hat(l,:)*E_tt(1,:)'))+(Rx_mag(m,:)-
(Rx_hat(m,:)*E_tt(1,:)')))/c); %time delay
                phi=K_tx*Rx_mag(m,:)-
K_tx*(Tx_hat(l,:)+Rx_hat(m,:))*(E_tt(1,:)+((Rx_hat(m,:)*(Rx(m,:)-
E_tt(1,:))')*E_tt_vel/c))';
                alpha=1-(Tx_hat(l,:)+Rx_hat(m,:))*(E_tt_vel/c)';
                E_TT_Data                =                E_TT_Data                +
exp(i*phi)*exp(i*W_tx*alpha*T).*ifft(S.*exp(-i*w*tau));
              end
            end
            I(g,h)=E_TT_Data*TT_Data';
          end
        end

   I_abs=abs(I);
   I_norm=I_abs/max(max(I_abs));
   I_tt=(I_norm-0.707); %applying -3dB thresholding
   I_tt=ceil(I_tt)*E_tt_vel_mag;
   [row,col]=find(I_tt);
   Vel_U(row,col)=E_tt_vel(1,1);
   Vel_V(row,col)=E_tt_vel(1,2);
   if nn==1
      I_tt_sum=I_tt;
   else
      I_tt_sum=I_tt_sum+I_tt;
   end
   nn=nn+1;
   end
end

figure
surf(E_tt_x,E_tt_y,I_tt_sum); %or I_norm*E_tt_vel_mag
%title(['velocity Vector [', num2str(E_tt_vel),']']);
colorbar;
hold on
quiver3(X,Y,I_tt_sum,Vel_U,Vel_V,Vel_W);
```

LIST OF REFERENCES

[1] M. Cheney and B. Borden, "Imaging moving targets from scattered waves," Institute of Physics Publishing on Inverse Problems, Vol. 24, April 2008.

[2] J. R. Guerci, *Space-time adaptive processing for radar*, Artech House, 2003.

[3] J. S. Bergin and P. M. Techau, "Multiresolution signal processing techniques for ground moving target detection using radar," EURASIP Journal on Applied Signal Processing, No. 47534, 2006.

[4] Y. L. Wang et al., "Space-time adaptive processing for airborne radar with various array orientations," IEE Proc Radar, Sonar Navig., Vol. 144, No. 6, pp. 330–340, December 1997.

[5] B. Friedlander and B. Porat, "VSAR: A high resolution radar system for detection of moving targets," IEE Proc Radar, Sonar Navig., Vol. 144, No. 4, pp. 205–218, August 1997.

[6] "Radar," class notes for PH 4274, Physics Department, Naval Postgraduate School, May 2008.

[7] M. I. Skolnik, *Introduction to radar systems*, 2nd edition, McGraw-Hill, 2001.

[8] B. Borden, *Radar imaging of airborne targets: A primer for applied Mathematicians and Physicists*, Taylor & Francis, 1999.

[9] M. Bertero and P. Boccacci, *Introduction to inverse problems in imaging*, pp. 81-86. Institute of Physics Publishing, UK, 1998.

[10] MAJ Tan Lu Pin, "Analysis of point spread function for imaging moving targets from scattered waves," Master's thesis, Physics Department, Naval Postgraduate School, December 2008.

[11] MAJ Teo Beng Koon, William. "Radar Imaging for Moving Target," Master's thesis, Physics Department, Naval Postgraduate School, June 2009.

THIS PAGE INTENTIONALLY LEFT BLANK

INITIAL DISTRIBUTION LIST

1. Defense Technical Information Center
   Ft. Belvoir, Virginia

2. Dudley Knox Library
   Naval Postgraduate School
   Monterey, California

3. Professor Andres Larraza
   Naval Postgraduate School
   Monterey, California

4. Professor Brett Borden
   Naval Postgraduate School
   Monterey, California

5. Professor Phillip E. Pace
   Naval Postgraduate School
   Monterey, California

6. Professor Yeo Tat Soon
   Director, Temasek Defence Science Institute
   National University of Singapore

7. Tan Lai Poh (Ms)
   Assistant Manager, Temasek Defence Science Institute
   National University of Singapore

8. Ng Chee Yong
   Defence Science and Technology Agency
   Singapore